Geomorphology 107 (2009) 300–315

Contents lists available at ScienceDirect

Geomorphology

journal homepage: www.elsevier.com/locate/geomorph

Evaluation of paleohydrologic models for terrestrial inverted channels: Implications for application to martian sinuous ridges

Rebecca M.E. Williams [a,*], Rossman P. Irwin III [b], James R. Zimbelman [b]

[a] Planetary Science Institute, 1700 E. Fort Lowell, Suite 106, Tucson, AZ 85719, United States
[b] Center for Earth and Planetary Studies, National Air and Space Museum, Smithsonian Institution, Independence Avenue at Sixth Street SW, MRC 315, P.O. Box 37012, Washington, D.C. 20013-7012, United States

ARTICLE INFO

Article history:
Received 11 July 2008
Received in revised form 22 December 2008
Accepted 23 December 2008
Available online 8 January 2009

Keywords:
Fluvial geomorphology
Mars
Hydrologic models

ABSTRACT

Fluvial systems can be preserved in inverted relief on both Earth and Mars. Few studies have evaluated the applicability of various paleohydrological models to inverted fluvial systems. The first phase of this investigation focused on an extensive (spanning ~ 12 km) inverted paleochannel system that consists of four sandstone-capped, carbonate-cemented, sinuous ridges within the Early Cretaceous Cedar Mountain Formation located southwest of Green River, Utah. Morphologic and sedimentologic observations of the exhumed paleochannels were used to evaluate multiple numerical models for reconstructing paleofluvial hydrological parameters. Another objective of the study was to determine whether aerial or orbital observations yield model results that are consistent with those constrained by field data. The models yield an envelope of plausible dominant discharge values (100–500 m^3/s), reflecting the limitations of the approach, and no single model can be used to reliably estimate paleodischarge. On Mars, landforms with attributes consistent with inverted channels have been identified. In spite of differences in the formation history between these martian landforms and the terrestrial analog described here, including potential differences in cement composition and the erosional agent that was responsible for relief inversion, these numerical models can be applied (with modification) to the martian landforms and yield an envelope of plausible values for dominant discharge.

1. Introduction

Relief inversion is an aspect of landscape evolution on both terrestrial (Pain and Ollier, 1995) and martian (e.g., Williams and Edgett, 2005; Williams et al., 2005; Pain et al., 2007) denuded surfaces, where materials deposited in topographic lows were or became more resistant to erosion than the surrounding terrain. Exhumation of martian terrains was identified in some of the earliest orbital images (Sharp, 1973; Soderblom et al., 1973) and is now recognized as a widespread process on Mars (Malin and Edgett, 2001). Inverted topography of fluvial landforms results when differential erosion preferentially strips away the less resistant valley or channel walls, leaving the original floor as a local topographic high. (We differentiate channels, the conduit through which water flows, from the larger-scale valley.) Several processes can lead to relief inversion, including cementation of the channel floor, armoring of the channel floor by coarse grains, and infilling by a more resistant material (commonly a lava flow).

Cemented, positive-relief channels are good environments for preservation of fluvial sediments, with exposures in three dimensions and retention of many attributes of the original channel form. The preservation of these sedimentary attributes, including grain size distribution and sedimentary structures, provides a record of the fluvial conditions during active flow and is useful for evaluating paleohydrological models. In contrast, lava-capped inverted valleys are the result of lava infilling of the valley, a process that obscures sedimentary structures in plan view. A lava flow may occupy both a fluvial channel and its surrounding valley floor such that morphometric observations of the inverted topography do not necessarily reflect the channel dimensions and formative discharge.

The motivation for this investigation stems from the recent recognition that fluvial landforms on Mars have a variety of preservation states (Williams and Edgett, 2005). In addition to the negative-relief valley networks first identified in Mariner 9 images (McCauley et al., 1972), some valleys are buried (e.g., Mangold et al., 2004) and others are preserved as ridge forms and positive-relief branching networks. In this report, the nongenetic term "sinuous ridges" will be used to refer to these landforms on Mars, although other terms have been adopted in the literature including "raised curvilinear features" (RCFs) (Burr et al., 2006; Williams, 2007). Over 200 sinuous ridge sites have been identified in meter- and decameter-scale images around the martian globe, covering areas ranging from tens to hundreds of square kilometers (Pain et al., 2007; Williams,

* Corresponding author. Tel.: +1 520 622 6300; fax: +1 520 622 8060.
E-mail address: williams@psi.edu (R.M.E. Williams).

0169-555X/$ – see front matter © 2009 Elsevier B.V. All rights reserved.
doi:10.1016/j.geomorph.2008.12.015

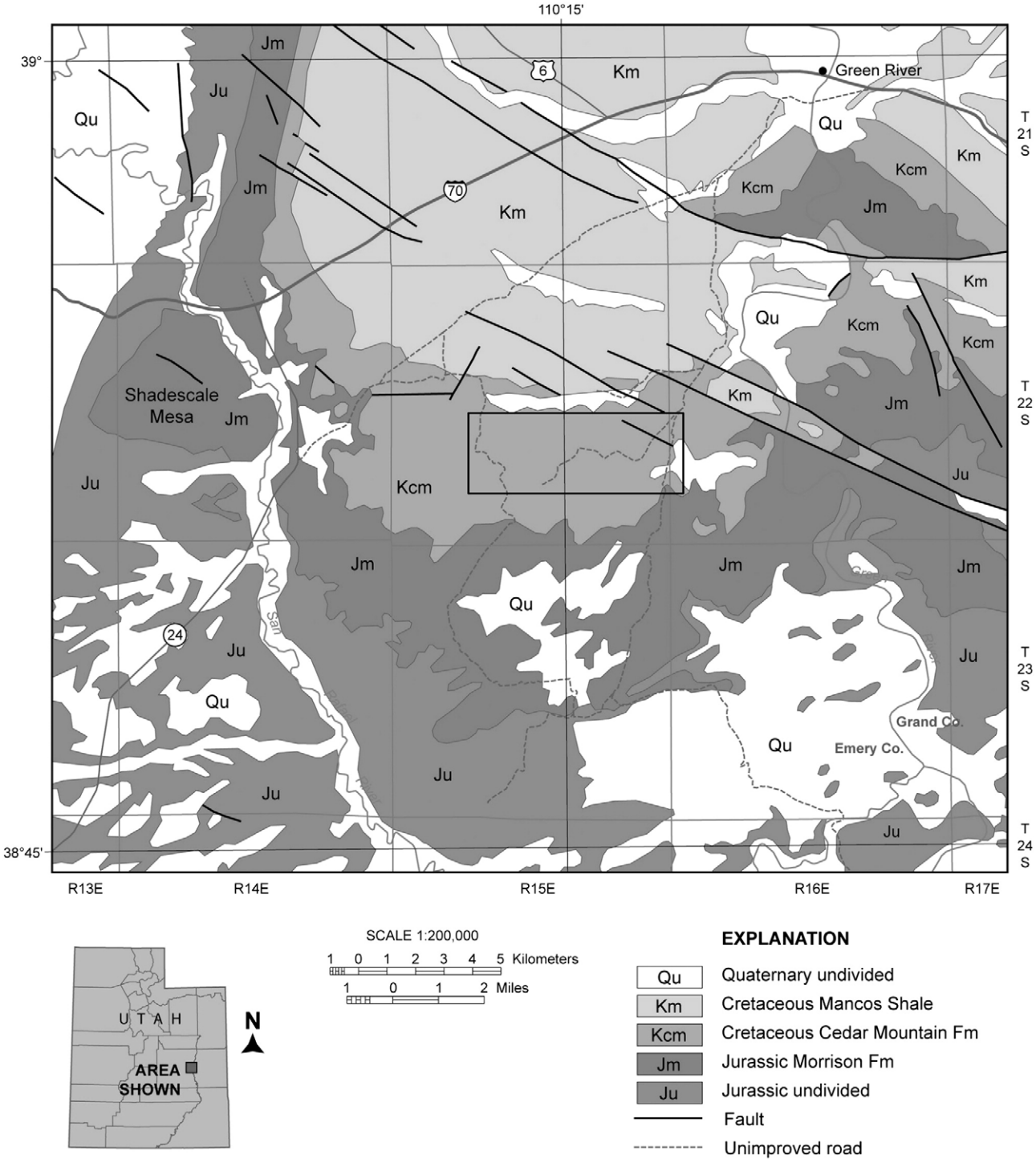

Fig. 1. Geologic map of the study region in east-central Utah. Inverted paleochannels are located in the Cedar Mountain Formation. Black box is approximate outline of Fig. 3, a portion of the study site.

2007). In contrast to valley networks, which are primarily found on the ancient cratered highlands, sinuous ridges are found on terrain with ages that span the entire geological history of the planet, from the Noachian to the Amazonian Periods, expanding the record of past water on Mars (Williams, 2007).

All published studies to date have interpreted martian sinuous ridges as fluvial in origin, but authors have differed on the water source. Based on their curvilinear and bifurcating appearance, continuity relationships with negative-relief valley networks, and similarity to terrestrial fluvial landforms, the sinuous ridges are interpreted to be the remnants of former fluvial channels formed by continually flowing water, now expressed in inverted relief (Moore and Howard, 2005; Williams and Edgett, 2005; Pain et al., 2007). Sedimentary structures that support this interpretation are evident in some of the martian sinuous ridges. For example, scroll bars are present in the putative deltaic deposit defined by cross-cutting sinuous ridges within Eberswalde crater (Malin and Edgett, 2003; Moore et al., 2003; Bhattacharya et al., 2005; Wood, 2006). In addition to precipitation-fed surface runoff (e.g., Moore et al., 2003; Moore and Howard, 2005), other scenarios for generating fluids have been proposed in the formation of these landforms, including impact-generated melt from ground-ice (Jerolmack et al., 2004), glacial

Fig. 2. Color aerial photomosaic (1 m/pixel) of study site location in eastern Emery County. Letters A–D refer to designations assigned by Harris (1980) for the four inverted paleochannel systems mapped in the Cedar Mountain Formation at this site. Image courtesy Virtual Utah (http://earth.gis.usu.edu/utah), Remote Sensing and GIS Laboratory, Utah State University, Logan.

meltwater or subglacial streams (eskers) (Howard, 1981; Kargel and Strom, 1992; Nussbaumer et al., 2003; McMenamin and McGill, 2005; Burr et al., 2006). The majority of the sinuous ridges have morphology consistent with open-channel flow, as examined in this study. Very few sinuous ridges, confined to specific regions on Mars (e.g., Argyre Planitia and Aeolis/Zephyria Plana; Kargel and Strom (1992) and Burr et al. (2008), respectively), are interpreted to be eskers primarily because they cross pre-existing topographic divides. Under this interpretation, these sinuous ridges would have formed in a closed and potentially pressured environment that is inconsistent with the terrestrial analog site investigated in this paper.

The diverse suite of sinuous ridges preserved on Mars documents a range of paleofluvial environments and attests to the complex fluvial history of the planet. The channel systems as observed today are the products of combined burial, exhumation, and degradation. Several studies (e.g., Moore et al., 2003; Fassett and Head, 2005; Irwin et al., 2005) have applied hydraulic models derived from the study of active fluvial systems on Earth to one or more of these inferred inverted martian landforms, even though few terrestrial studies have documented the applicability of such models to inverted channels. In this study, we evaluate the applicability of both empirically and theoretically derived paleohydrologic models for modern streams to cemented inverted channels based on analysis of field data for inverted paleochannels in east central Utah. Future phases of this research will investigate other agents of inverted relief in fluvial systems, including lava infilling. Results of this study can be used to assess the magnitude of fluvial activity in inferred inverted channels on Mars.

2. Study region

Multiple exhumed paleochannels are found in parts of the Colorado Plateau. Following uplift of the region in middle to late Cenozoic time, erosion, dominantly by the Colorado River and its tributaries, stripped away younger strata, revealed Late Jurassic and Early Cretaceous paleochannel sediments at several sites in east central Utah (e.g., Williams et al., 2007). The present-day arid climate has inhibited the development of thick soil horizons and pervasive vegetative cover, leaving these fluvial deposits exposed. The focus of this investigation is several Early Cretaceous inverted paleochannel segments each spanning several kilometers in length and rising ~30–40 m above the surrounding terrain, located 11 km SW of Green River, Utah (Figs. 1 and 2). These fluvial sediments were first buried by marine sediments from a Late Cretaceous inland sea. Burial history models for the region indicate that ultimately 2400 m of sediment overburden was laid down in various depositional environments

Fig. 3. Oblique aerial photograph of two paleochannel sections looking northward. Channel segments did not form simultaneously, and the bifurcation marked by black arrows is two segments at different topographic and stratigraphic levels. The inverted paleochannel segment from top to bottom (north to south, segment D) in image is stratigraphically higher than the shorter paleochannel segment that extends to the right (east, westernmost section of segment B). Image width is ~3 km.

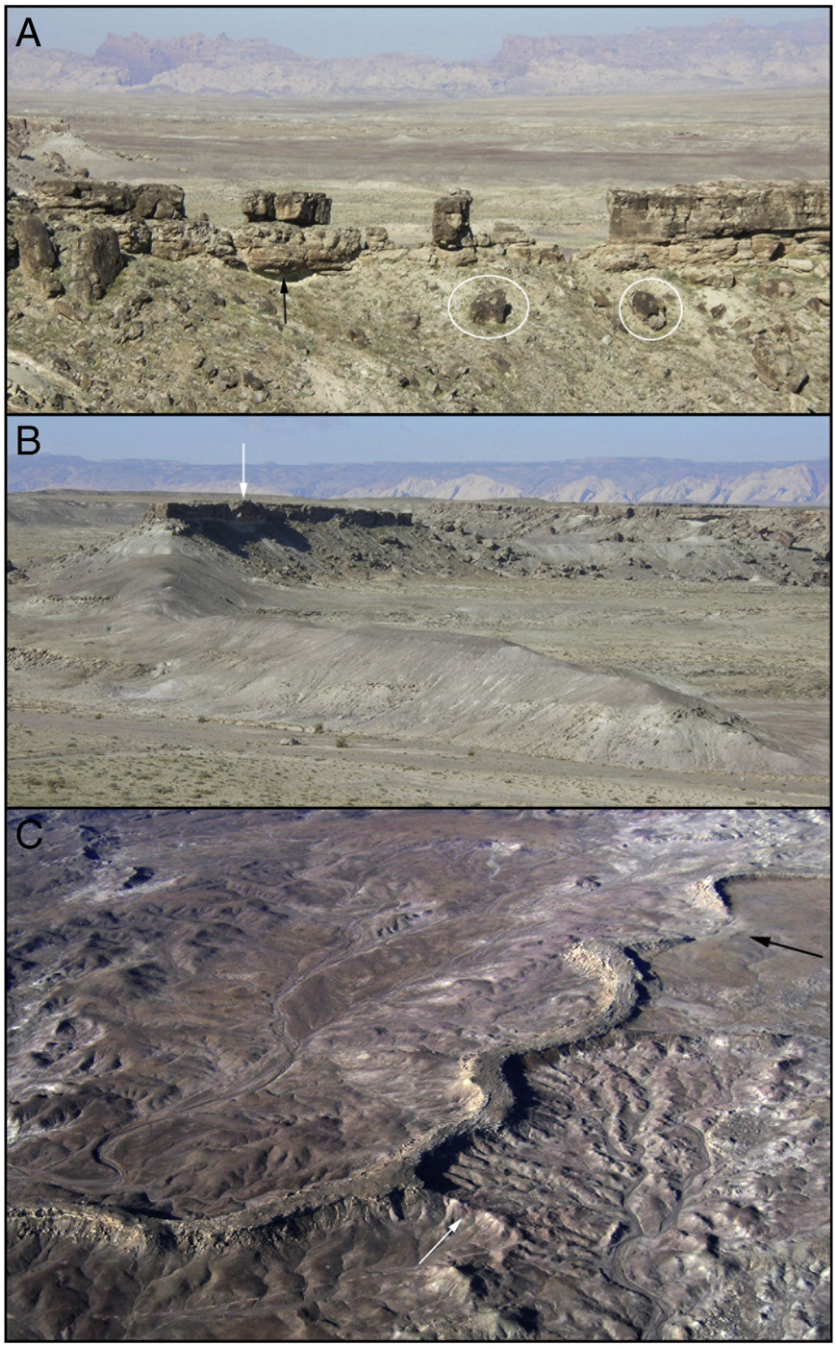

Fig. 4. (A) Blocks of the inverted paleochannel caprock are locally eroded, producing gaps along the former channel course. In some places, undermining (black arrow) of the underlying poorly indurated mudstone is evident. Ultimately paleochannel blocks (circled) are transported downslope by mass wasting. (B) Cemented fluvial sediments form a capstone (white arrow). Where the capstone has been removed along a portion of segment A, the underlying mudstone that had been protected from erosion indicates the original flow path. (C) Oblique aerial photograph to the SW of a sinuous section of channel A. A modern, well-developed drainage network (bottom right) is undermining less indurated material beneath the cemented fluvial sediments and has locally removed the capstone (water gap marked by black arrow at top right). Tributaries (white arrow at center bottom) to the main trunk channel are rarely preserved at the site. Image width in foreground is ~1800 m. Illumination is from the upper left.

(Nuccio and Condon, 1996; Nuccio and Roberts, 2003). Based on this reconstruction model, long-term erosion rates for the region (0.06 m/kyr) can be used to determine the maximum surface re-exposure age for this site at ~650,000 years (present relief divided by erosion rate yields surface exposure age). (The paleochannel sandstones resisted erosion once they were re-exposed at the surface, and erosion of the surrounding mudstones produced the ridge form observed today.) However, this number is likely an overestimate as some studies suggest that uplift was more rapid in the last few million years (e.g., Sahagian et al., 2002) and increased precipitation associated with the Pleistocene climatic changes in the region would enhance erosion. Consistent with the latter point, estimated incision rates for the Colorado River and its tributaries over the past million years are three to eight times higher than the estimated long-term erosion rate (e.g. Davis et al., 2001; Hanks et al., 2001; Marchetti and Cerling, 2001; Willis and Biek, 2001; Pederson et al., 2002).

The field site has several sandstone- and conglomerate-capped sinuous ridges (the fluvial capping layer is up to 10 m thick) that occur in the Ruby Ranch Member (shale and maroon mudstone deposited in Aptian to middle Albian time) of the Cedar Mountain Formation (Elder and Kirkland, 1993; Kirkland et al., 1998). The base of this unit is defined by a 1–10 m thick, nodular calcrete horizon that formed

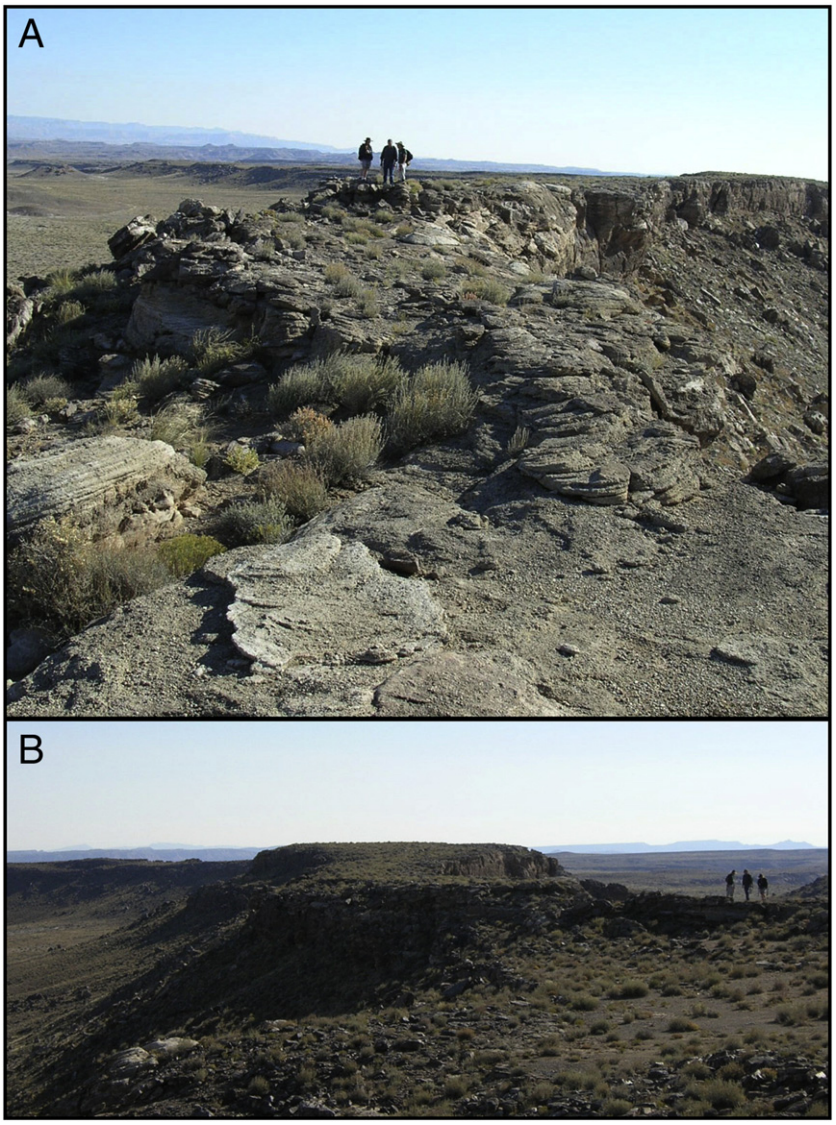

Fig. 5. Two views along segment B. (A) Foreground is a point-bar deposit, which typically have irregular meter-scale undulations at the surface. Channel fill deposits are preserved in the background at right with vertical cliffs. (B) Channel width is more uniform with channel fill deposits that typically exhibit a flat surface.

during an arid to semiarid climate (Currie, 1998). At the time of fluvial deposition, the climate was transitioning from a seasonal semiarid climate to a more humid one (Currie, 1998; Demko et al., 2004; Al-Suwaidi et al., 2007). Groundwater flows more easily through the porous channel deposits than through the mud overbank deposits. Cementation of the channel deposits may have occurred via evaporation of groundwater that concentrated calcium carbonate and other minerals at the surface during the dry season, leading to indurated fluvial deposits (Harris, 1980). Alternatively, carbonate cementation may have occurred during post-depositional diagenesis (e.g., Arakel, 1986; Khalaf, 1990; Spötl and Writght, 1992). In addition to carbonate cement, Lorenz et al. (2006) reported localized quartz cement (grain-coating and pore-filling) binding the fluvial sediments.

Harris (1980) mapped the exhumed sandstone to conglomerate ridges as four separate channel systems that he denoted segments A–D (Fig. 2). We refer to these ridges as paleochannels or simply channels, following the definition of Stokes (1961, p. 165): a body of clastic material, regardless of size and shape, generally sandstone and/or fine conglomerate, originally deposited by rapidly flowing water in an ancient stream course, which has internal structures indicating the direction of sediment course. These single-thread channels are generally linear, although some reaches exhibit low sinuosity with sinuosity ratios between 1.2 and 1.5 (Harris, 1980). Fluvial activity within these channels may not have been contemporaneous, as two of the exhumed channels exhibit a clear superposition relationship (Fig. 3).

Paleochannels are discontinuously preserved in discrete sections. We infer that some in-line channel sections were once connected, with the longest channel (B) extending ~8 km. Erosion of the underlying mudstone leads to undermining of the channel (caprock) which breaks down into blocks that are transported downslope by mass wasting (Fig. 4A). Where the caprock has been removed, the underlying mudstone develops a rounded crest (Fig. 4B). Incision of modern streams has also created gaps along the paleochannel course (Fig. 4C).

Exhumed paleochannel surfaces at this site preserve both sand-sized channel-fill deposits and gravel-rich point-bar deposits, which are concentrated on the inside inflections of channel bends. The caprock preserves an aggrading channel bed, and the exposed strata represent deposits from multiple flow events. Weathering of point-bar deposits produces an irregular surface, nonvertical scarps bounding the caprock, and variable channel widths; whereas channel-fill deposits erode into a relatively smooth surface and vertical cliffs, with better preservation of the original channel width (Harris, 1980; Fig. 5).

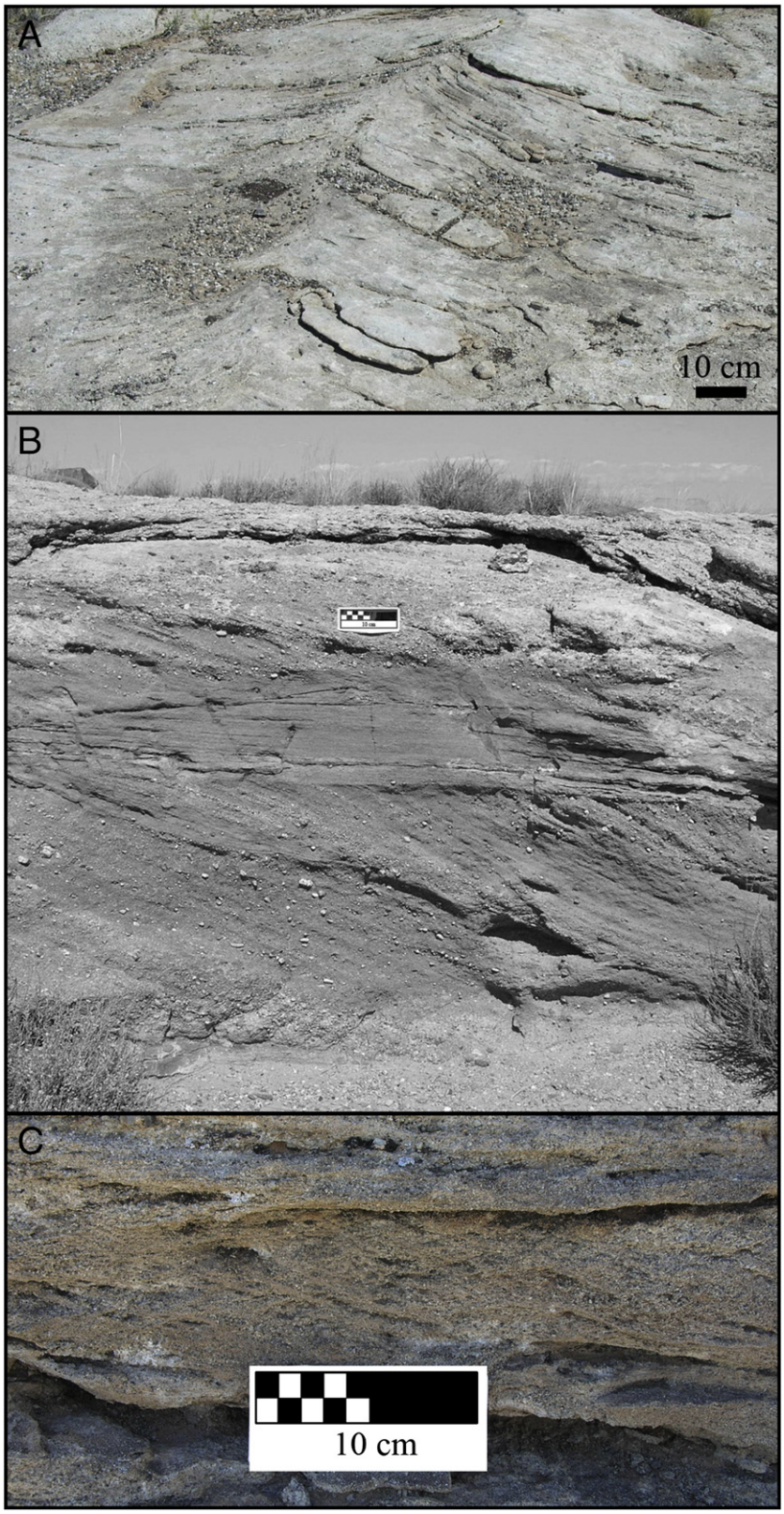

Fig. 6. Examples of sedimentary structures in paleochannel segment B. (A) Surface exposure of cross-beds with 10-cm scale bar. Flow direction is into the page. (B) Vertical exposure of ~1 m with graded bedding in trough cross-beds at base, horizontal stratification at mid-section, and channel-fill deposits at top. Scale bar is 10 cm. (C) Climbing ripples exposed in vertical exposure of point-bar deposit. Ripple marks are rarely found on paleochannel surfaces.

Cross-bed sets in the sandstones are expressed both in vertical exposures and on the ridge surfaces, in the latter case as scalloped textures that are broadly concave in the downstream direction (Fig. 6). The paleocurrent direction to the east and north is consistent with the direction of the encroaching Western Interior Seaway (Harris, 1980). On the basis of composition and direction of sediment transport, the source rocks were located southwest of the study site with potential source regions including the San Francisco and

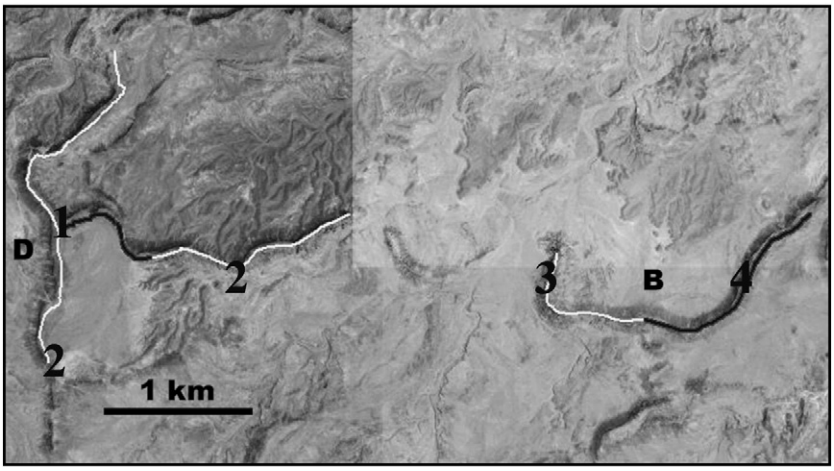

Fig. 7. The path of longitudinal profile data acquisition on inverted paleochannels is highlighted in white on mosaic of aerial photographs. Note that portions of data marked black on figure were excluded from the study because of proximity to the fault zone (eastern section) and slope counter to field paleflow indicators (western section). Along channel 'B', there is a U-shaped section at mid-image where the caprock has been removed, so this area was not part of the survey. Numbers mark approximate location where grain size surveys were conducted; results reported in Table 1.

Wah Wah Mountains thrust sheets in southwestern Utah, and the Sevier belt of southeastern Nevada (Yingling and Heller, 1992; Currie, 1998).

Regional structural dip is a few degrees to the NE (Doelling, 1994; Lorenz et al., 2006). Paleochannel sections in the far eastern portion of the study region are cross-cut by WNW-striking faults with offsets of 5–10 m (Williams and Hackman, 1971). These faults are laterally traceable to a system called the Salt Wash faults that were active during early Tertiary and Quaternary time, and possibly during middle Cretaceous time as well (Doelling, 1994; Shipton et al., 2004).

Lorenz et al. (2006) documented several families of vertical extension fractures in the inverted paleochannels. Pervasive throughout the inverted paleochannels are fault-parallel fractures that consistently strike WNW regardless of the local axial orientation of the inverted paleochannel segments, reflecting the orientation of faults located to the east. These fractures likely formed simultaneously with the local faults in response to vertical overburden stress. Valley-wall fractures are the youngest and form as a result of gravitational forces and erosion of the underlying mudstone. The underlying ductile, muddy strata spreads laterally under the weight of the paleochannel caprock to generate the fractures that trend subparallel to channel margins (Lorenz et al., 2006). These fractures are readily discernible in aerial photographs, with trace lengths of several tens of meters and open apertures up to several meters.

3. Methods

3.1. Measurements

The primary objective of field work was to obtain input parameters for the paleohydrologic models (described in Section 3.2). Secondarily, the suite of field measurements was compared to data derived from aerial photographs, as an appraisal of measurements obtained from remotely sensed data. The following sections describe the methods employed in this study.

The topographic survey obtained direct measurements of the present-day width and slope of inverted channels termed "B" and "D" by Harris (1980) (see Fig. 7 for location). High-precision topographic measurements of inverted channels were made using the Trimble 4800 Total Station, a carrier-phase Differential Global Positioning System (GPS). Differential correction of GPS data allows positions to be determined relative to the base station with a horizontal accuracy of 1–2 cm and vertical accuracy of ~2–4 cm. Longitudinal profiles were constructed from DGPS data collected at bedrock exposures along the course of the inverted channel (Fig. 7). Cross-sectional profiles were taken at a few locations along each channel to document its shape and measure channel width.

To determine the distribution of grain size in the channel, we adopted the Wolman pebble count method, which relies on measurements from a sample of surface sediments (Wolman, 1954). The intermediate axis of each particle in the sample is measured by passing the particle through a handheld sieving device, a gravelometer, that has slots in half phi (ϕ) increments. For particles cemented in place, the gravelometer was held up to the particle to assess the appropriate slot size. The Krumbein phi (ϕ, mm) scale (Krumbein and Sloss, 1963, a modification of Wentworth, 1922) is defined as

$$\phi = -\log_2(P/P_o) \quad (1)$$

where P is the particle diameter in mm, and P_o is the reference particle diameter of 1 mm. To create a representative sample, the median diameter of each particle touched by the toe of one foot is measured at every step in several passes across the channel. A sample size of 100 particles was acquired to identify the mean or median diameter (D_{50}, m) and the diameter at one standard deviation from the mean (D_{16} and D_{84}). All surface sampling methods systematically underrepresent the finer sediment in the grain size population (Wolman, 1954). Sample size analyses were conducted at multiple points along the channel.

Aerial photos from the U.S. Geological Survey were obtained online from http://terraserver-usa.com/(courtesy of Microsoft). Channel dimensions were measured using the software USAPhotoMaps (http://jdmcox.com/). Aerial photos (resolution of 1 m/pixel) are comparable to high-resolution orbital image data from Mars such as the Mars Orbiter Camera (MOC, 0.5–12 m/pixel; Malin et al., 1992, 1998) and the High Resolution Imaging Science Experiment (HiRISE, 0.25–1.3 m/pixel; McEwen et al., 2007).

3.2. Paleohydrologic models

In this study, we expand upon the methodology of Maizels (1987), who examined inverted or "raised" channels in Oman that were part of an alluvial fan complex (see also Maizels, 1983). This study investigates the applicability of paleohydraulic models to exhumed meandering channels. Two approaches (micro- and macro-scale) to paleodischarge estimation were employed, and an envelope of discharge estimates was produced based on several different models

Table 1
Field site characteristics of various models used in this study.

Method	Eq.	Location	Bed material	Grain size	Grain size (m)	Slope range
Strickler	7	Germany, Switz.	Gravels	D_{50}	<0.25	0.00004–0.025
Limerinos	8		Gravel to boulder	D_{84}	0.02–0.75	0.00068–0.024
Bray	9		Gravels			0.00022–0.015
Jarrett	10		Cobble to boulder	D_{84}	0.1–0.8	0.002–0.052
Hey	13	United Kingdom	Gravel to cobble	D_{84}	0.046–0.25	0.0090–0.031
Griffths	14	New Zealand	Gravel to boulder	D_{50}	0.013–0.301	0.000085 to 0.011
Bathurst	15		Cobble to boulder	D_{84}	0.113–0.740	0.004–0.04
Kleinhans	16	190 rivers worldwide	Sand to gravel		0.00015–0.1887	0.0000217–0.091
Carlston	18	Central US	N/A	N/A	N/A	N/A
Schumm	19	US, Australia	Clay to sand			
Osterkamp & Hedman	22	Missouri R. basin	Silt to cobble	D_{50}	2×10^{-5} to 0.25	0.000060–0.028
This study		Utah	Sand to gravel		0.002–0.045	0.001–0.002

within each approach. This method enables an exploration of parameter space and mitigates many of the limitations and errors in both model assumptions and field measurements. Examining this suite of models for the terrestrial analogs provides ground truth and validation in applying these models to martian inverted channel systems. Hydrologic models that require only remotely sensed data may be applicable to sinuous ridges on Mars (if the equations are scaled for gravity), but many of these models involve simplifying assumptions (e.g., grain size, bed roughness, or width/depth ratio as a function of bank resistance) that are unconstrained in martian settings, making multiple models useful in determining a range of possible formative discharges.

All of the paleoflow equations below are based either on hydraulic relationships between sediment and flow parameters in present-day streams or flumes, or geomorphic relationships between channel morphology, channel sediments, and discharge measured in modern rivers (Table 1). The hydraulic or micro approach (Jopling, 1966) provides estimates of short-term (or instantaneous) velocity or discharge conditions as a result of local adjustment of hydraulic geometry around a mean or equilibrium channel condition. The geomorphic or macro approach indicates the development of longer term equilibrium or quasi-equilibrium conditions between catchment, channel, and flow parameters (e.g., Langbein and Leopold, 1964). All models use metric units. Initial inputs of model parameters are derived directly from field measurement and image datasets or computed based on field measurements, as described below.

3.2.1. Micro approach based on hydraulic-sediment relationships

The most basic equation in open-channel (free-surface) flow hydraulics is the continuity equation for discharge, Q (m^3/s)

$$Q = wHv \tag{2}$$

where w is channel width (m), H is flow depth (m), and v is the average flow velocity (m/s). The concept of flow equilibrium is formalized in this equation, as a change in one independent variable is matched by a mutual adjustment of other variables in order to maintain dynamic equilibrium.

Variations in methods of determining the input parameters in Eq. (2) result in several different models for estimating paleodischarge. Paleochannel width measurements can be directly obtained in the field or from satellite images, although incomplete preservation or destruction of the paleochannel may result in an underestimation of this parameter, or lateral migration could yield a sandstone caprock that is wider than the active paleochannel was at any one time. Paleoflow depth and velocity can be estimated based on the threshold shear stress at which bed particles begin to move, as described below.

3.2.1.1. Estimation of flow depth. The Shields (1936) criterion represents the threshold shear stress τ_t ($N\ m^{-2}$) at the point when the bed particles begin to move, which can be used to determine a minimum or threshold flow depth H_t (m) by

$$H_t = \tau_t / \gamma S \tag{3}$$

where S (m/m) is the former hydraulic gradient and γ (N/m^3) is the specific weight of water (density ρ (kg/m^3) times gravitational acceleration g (m/s^2)). Threshold shear stress is calculated using the semi-empirical function

$$\tau_t = \theta(\gamma_s - \gamma)\, D \tag{4}$$

where θ is the Shields coefficient (dimensionless threshold shear stress), γ_s is the specific weight of sediment, and D (m) is the size of the bed roughness element (the largest particle size, assumed to be D_{84} here) where D is larger than ~0.2 mm. For reference, typical density values are $\rho_s = 2650$ kg/m^3 for quartz sand, $\rho = 1000$ kg/m^3 for clear water, and $\rho = 1165$ kg/m^3 for 10% suspended sediment concentration. In this study, clear-water conditions were assumed. The coefficient θ is assumed here to have Shields' original value of 0.056; however, this value may vary from as low as 0.01 to as much as 0.1 depending on sediment sorting, particle shape, and particularly on the looseness of packing of the boundary (Church, 1978), with typical values ranging from 0.03 to 0.06 (Komar, 1988; Knighton, 1998). Over- or underestimating the flow depth not only affects the discharge but also the velocity through the roughness equation (Eqs. (5) and (6) below).

3.2.1.2. Estimation of paleoflow velocity. Under the assumption of steady, uniform (i.e. constant depth) flow in a channel that has a rigid boundary (i.e., flow conditions up to bed motion), the threshold mean flow velocity, v_t (m/s), can be computed based on resistance coefficients and channel geometry by two widely used methods. The first employs the Manning roughness coefficient, n:

$$v_t = \left(R^{0.67} S^{0.5}\right) / n \tag{5}$$

and the second uses the Darcy–Weisbach friction factor, f:

$$v_t = \left[(8gR\ S)/f\right]^{0.5} \tag{6}$$

where R (m) is the hydraulic radius (ratio of flow cross-sectional area to wetted perimeter). The threshold mean flow velocity is a function of the size of bed particles that have been entrained, as evident in the equations for determining the resistance coefficients n and f below (Eqs. (7)–(11) and (13)–(16)).

Unlike the empirical Manning-type equation, the Darcy–Weisbach equation uses a dimensionless friction factor, has a sound theoretical basis, and explicitly accounts for the acceleration from gravity; moreover, the relative roughness does not influence the exponents of hydraulic radius (Raudkivi, 1967) and slope (Liu and Hwang, 1959). For these reasons, the Darcy–Weisbach equation is preferred over the Manning approach (Silberman et al., 1963, Kleinhans, 2005). The objective of this study is to evaluate multiple hydraulic models, and we examine versions of both the Manning and Darcy–Weisbach equations.

The Manning relationship for open-channel flow (Eq. (5)) was originally formulated based on empirical observations, but it recently was derived theoretically using the phenomenological theory of turbulence (Gioia and Bombardelli, 2002). Manning roughness

coefficients have been related to field observations in natural streams (Arcement and Schneider, 1989). Algebraic manipulation has been used to relate n and f (e.g., Bettess, 1999; Wohl, 2000) and various relationships have been proposed between the resistance coefficients (n,f) and sediment grain size. (In this study, D_{84} was universally used for grain size although it is most appropriate for grain roughness on the channel bed, and D_{50} may be more relevant to critical shear stress for transport (Parker et al., 1982). The adoption of D_{50} in relevant equations minimally altered the derived values.) Strickler (1923) assumed that grains were the dominant roughness element (i.e. no bedforms) and used flow data from pipes and several European rivers to relate the Manning roughness coefficient n to D_{50}:

$$n = 0.039 D_{50}^{0.167}. \quad (7)$$

Limerinos (1970) related the roughness coefficient to flow depth and D_{84}:

$$n = \left(0.113 R^{0.167}\right) / \left(1.16 + 2.0 log(R / D_{84})\right) \quad (8)$$

based on data from low gradient channels with bed material comprised of small gravel to medium-sized boulders. A similar relationship to Eq. (8) was derived by Bray (1979), who examined gravel-bed rivers:

$$n = \left(0.113\ R^{0.167}\right) / \left(1.09 + 2.2 log(R / D_{84})\right). \quad (9)$$

Jarrett (1984) derived an equation for shallow (<2.2 m), steep-gradient flows:

$$n = 0.032 S^{0.38} R^{-0.16}. \quad (10)$$

The Darcy–Weisbach friction factor, f, in fully developed, uniform flow was estimated by Colebrook (1939):

$$\left(1 / f^{0.5}\right) = C log(aR / k_s) \quad (11)$$

where $C = 2.3$ ($\kappa / 8^{0.5}$), κ is the von Karman constant (0.4), k_s is the roughness height of the channel surface (here approximated by the representative grain size, D_{84}, as was done in Maizels (1987)), and a varies from 11.1 (infinitely wide channels) to 13.46 (circular pipes) depending on channel geometry (Keulegan, 1938). The value for a may be determined graphically (Hey, 1979) or from

$$a = 11.1 (R / H_{max})^{-0.314} \quad (12)$$

(Thorne and Zevenbergen, 1985). Eq. (11) was developed based on experimental studies of laminar and turbulent flow in pipes with a range of roughness and aperture size (Colebrook and White, 1937; Colebrook, 1939). Thus, Eq. (11) represents only the skin roughness of the surface material and does not take into account roughness from bedforms, bends, or flow nonuniformities found in the field. Therefore, approximating the roughness height with the representative grain size is an appropriate assumption.

Examination of regression equations for the Darcy–Weisbach friction factor f based on field data will demonstrate the effect of friction from other sources in natural channels. Hey (1979) developed an equation based on 21 straight, gravel-bed rivers in the United Kingdom and determined that the roughness height, k_s, is best approximated by $3.5 D_{84}$ in coarse-grained (gravel and cobble) natural channels with width/depth ratios > 15:

$$\left(1 / f^{0.5}\right) = 2.03 log(aR / 3.5 D_{84}). \quad (13)$$

Griffiths (1981) used a gravel-bed river data set from New Zealand to formulate an estimation of f:

$$\left(1 / f^{0.5}\right) = 0.76 + 1.98 log(R / D_{50}) \quad (14)$$

Bathurst (1985) developed an empirical equation for the friction factor in steep, boulder-bed rivers:

$$(8 / f)^{0.5} = 5.62 log(R / D_{84}) + 4. \quad (15)$$

Kleinhans (2005) derived a roughness parameter based on 190 rivers that encompassed a range of planforms (straight, meandering, and braided), bed sediment sizes (sand and gravel), and river sizes (small-scale streams to the Mississippi River), including perennial rivers as well as catastrophic flood channels:

$$(8 / f)^{0.5} = 2.2 (H / D_{50})^{-0.055} S^{-0.275}. \quad (16)$$

Kleinhans (2005) reported that uncertainty for computed flow velocity using this regression is a factor of 3.

Altogether, nine models of paleovelocity (Table 1) with input parameters that include flow depth or (its assumed equivalent) hydraulic radius, slope, and sediment size are outlined above. Note that for wide, shallow flows (i.e. width/depth ratios ≥ ~15), the hydraulic radius, R, is commonly replaced by flow depth, H. This simplifying assumption was adopted in this study. Uniform flow conditions are rarely observed in nature, but this assumption is generally adopted to simplify computations. Natural rivers with slopes < 1.5% typically experience subcritical flow (Church, 1992; Rosgen, 1994), an assumption that can be assessed based on field observations and computation of the Froude number (see Section 4.2 for further details).

3.2.2. Macro-approach based on empirical discharge-form relationships

The equations adopted here are empirical functions relating meander planform and channel morphological measures to discharge. Many of these relationships require determination of meander wavelength, L_M (m), radius of meander curvature, R_C (m), and bankfull channel width, w. Hence, major sources of error arise where former channel morphology is not well preserved. Several of the equations are for bankfull discharges with a recurrence interval of 1–2 years. Floods of this magnitude appear to control alluvial channel dimensions in many terrestrial humid regions, but limitations to this relationship are noted (Knighton, 1998, pp. 162–167).

Carlston (1965, modified by Williams, 1984a) established an empirical relationship between meander wavelength and floods with a recurrence interval of 1.5 years ($Q_{1.5}$),which are assumed to be the dominant discharge for streams in the central USA, such that

$$Q_{1.5} = 0.011 L_M^{1.54}. \quad (17)$$

Williams (1984a) related bankfull channel width and maximum flow depth to bankfull discharge, defined as $Q_{2.33}$, based on data collected by Schumm (1972) for semiarid and subhumid stable alluvial channels that transport clay to silt particles in the USA and Australia:

$$Q_{2.33} = 2.66 w^{0.9} H_{max}^{0.68}. \quad (18)$$

We assume that the threshold depth, H_t, is equivalent to the maximum channel depth (H_{max}, elevation difference between banktop and thalweg), which will result in an underestimation of bankfull discharge.

Williams (1984a,b) provided two functions that relate channel width and meander radius of curvature to the maximum instantaneous discharge (Q), which more closely matches the types of discharges predicted by the threshold shear stress approach. Williams (1984a,b) found for 19 meandering rivers in Sweden that

$$Q = 1.0 w^{1.3} \quad (19)$$

for 1.8 m ≤ w ≤ 67 m, and

$$Q = 0.28 R_C^{1.38} \quad (20)$$

for 8 ≤ R_C ≤ 169 m. Note that Eqs. (19) and (20) are only applicable for low-sinuosity channels.

Osterkamp and Hedman (1982) developed multiple empirically derived relationships between discharge and channel width based on data collected from various reaches along a large-scale drainage

system, the Missouri River basin. The majority of the data was obtained for sand-bed channels with sand or silt banks. Their equations are applicable to perennial alluvial streams. For this study, we used their overall empirical function that relates channel width w to discharge Q_2 (a flood with a recurrence interval of 2 years):

$$Q_2 = 1.9w^{1.22}. \quad (21)$$

4. Results

4.1. Input parameters

Accurate determination of the paleohydraulic model input parameters, such as flow cross-sectional area, former energy gradients, and maximum particle size, is complicated by multiple geologic processes that have operated on the fluvial deposits since the channels were active. Here we discuss how input values were determined based on field observations. Maizels (1983, 1987) discusses in additional detail the sources of error and problems inherent in reconstruction of paleochannel parameters.

4.1.1. Grain size

Field work focused on paleochannel segments B and D within the study site (Fig. 7). Grain size surveys were typically conducted at point bar locations where the coarsest fragments were deposited. Site B4 also included channel fill material (i.e., bedform cross-bed sets rather than point bar deposits) and therefore had finer grained clasts than were recorded at the other survey sites. Clasts measured in the grain size surveys were largely in the medium (8–16 mm) to coarse (16–32 mm) gravel size range (Table 2; Fig. 7). Decimal values reflect the binning of clasts into half-phi (ϕ) increments. Grain size results from the coarsest survey points (locations B1 and D2) were used in the paleohydraulic models.

We assumed that the measured grain sizes represent the coarsest grains entrained in the flows. This assumption appears valid given a) the size consistency of the coarsest particles (gravels) found at multiple survey points and within vertical cross sections of channel fill, b) that many of the coarser grains are cemented components of the fluvial caprock, and c) that the channel fills are surrounded by finer-grained (silt to sand) material. The channels incised a fine-grained sedimentary deposit (now mudstone), and the channel fill was buried by fine-grained marine sediments; therefore contamination by coarser particles not transported in the flows (i.e. weathered out from overburden) appears to be minimal.

4.1.2. Width

Channel width measurements were obtained in the field and on 1-m/pixel aerial photographs. Width was measured in the field at 18 points along channels B and D, spaced 100–200 m apart (Table 3). In addition, channel width measurements were acquired at ~100-m intervals from the aerial photographs (Table 4). Measured channel width values at the same site using these two methods are in good agreement, with values generally differing by <5 m. However, measurements made with aerial photos are susceptible to poor illumination conditions, and margin edges can be difficult to discern. In this study, one third of the measurements had large discrepancies (>5 m) between field and aerial photo measurement primarily because of channel margin shape (a rounded channel margin associated with point-bar deposits in contrast to the near-vertical margin of channel fills). In addition, a few width measurements were made at meander inflection points, which are locations of minimal channel migration in meandering rivers, and these widths ranged from 50–75 m.

The range of width values reflects incomplete preservation and/or destruction of the paleochannel, as well as the type of channel deposit. The lower width values appear to reflect poor preservation (incision and headward extension of modern drainage networks into the ridges, leaving narrow ridge outcrops), while maximum values may record lateral migration of the channel and overestimate the active channel width. Channel preservation is affected in part by the type of fluvial deposit along the course with point-bar deposits exhibiting a greater range of widths than sections that are exclusively channel fill deposits (Harris, 1980). Generally, the widest channel sections are preserved in areas farthest from and/or least affected by modern drainage (Fig. 4C).

The relative uniformity of preserved maximum channel widths evident in planview along much of the former channel course suggests that these are approximately equivalent to the original widths of the channel fill deposits (Figs. 2 and 6B). (This along course uniformity is not represented in the survey data, which was designed to be acquired at regular longitudinal spacing and therefore included measurements at locations that were wider or narrower than the approximately constant width in some sections.) With the variability of channel width measurements reflecting subsequent erosion (underestimate) and channel migration (overestimate), a representative value of original channel width for paleohydraulic models was assumed to be the third quartile of measured maximum channel width.

4.1.3. Depth

In this study, flow depth is computed based on the threshold shear stress for sediment transport described above (Eq. (3)). Inverted paleochannel deposits can preserve evidence of flow conditions that provide a check on the computed threshold flow depth, but the threshold shear stress offers a more precise estimate. The delineation of flow depth in the vertical section of a paleochannel deposit is not straightforward and provides merely a minimum boundary condition. Paleochannel deposits are sediments deposited in a shifting and/or aggrading channel (Schumm, 1972). Field investigation of flooding events demonstrates that the scour of a channel during floods is not significant in sand bed rivers (Colby, 1964a,b). A pebble layer may indicate the depth of scour (Livesey, 1963). In the absence of stratigraphic evidence for multiple flow events, the thickness of sediment deposits between pebble layers can be used as a proxy for minimum flow depth. Lenticular channel fills and fining upward sequences (e.g., Fig. 6) can be used as a direct estimate of flow depth and were measured to range from 0.5–1 m. Although the preserved

Table 2
Grain size survey results.

Location	Range (mm)	$\bar{x} \pm \sigma$ (mm)
Channel B1[a]	8–32	16 ± 4
Channel B2	8–22.6	14 ± 4
Channel B3	8–22.6	15 ± 4
Channel B4	2–22.6	9 ± 7
Channel D1	5.6–22.6	11 ± 4
Channel D2[a]	16–45	23 ± 5

[a] Data used in paleohydraulic models.

Table 3
Channel width based on field measurements.

Location	Data points	Range (m)	$\bar{x} \pm \sigma$ (m)
Channel B	10	23–89	57 ± 25
Channel D	8	17–66	38 ± 18

Table 4
Maximum channel width based on aerial photograph measurements.

Location	Data points	Range (m)	$\bar{x} \pm \sigma$ (m)
Channel B	22	33–85	58 ± 14
Channel D	22	23–125	55 ± 20

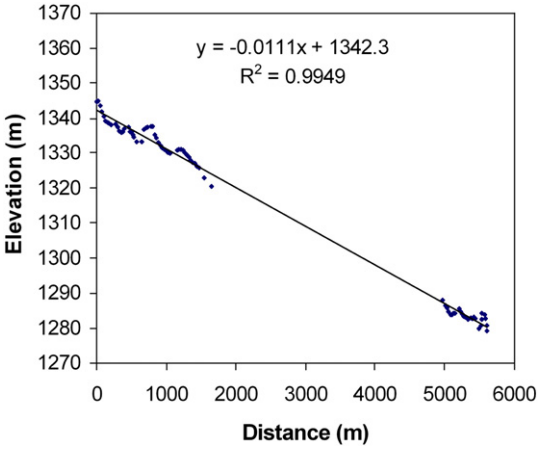

Fig. 8. Composite longitudinal profile for two sections of channel B from west to east. Although some of the meter-scale variability along the channel course may be from localized fault offsets, the overall fit to data is quite good ($R^2 = 0.99$). The channel is poorly preserved in the intervening section and no topographic data were collected. See Fig. 3 for location.

fluvial deposits are subject to subsequent erosion and therefore incomplete, an assessment of modern streams determined that the expected preservation fraction (preserved thickness/actual mean depth) is 60–70%, indicating that use of the preserved sedimentary deposit does not lead to a severe underestimation of the actual flow depth (Paola and Borgman, 1991). Thus, inferred flow depths from this method range from 0.7 to 1.7 m.

Cross-bedded units indicate that the channel did not typically remobilize the previously deposited sediments to any great depth. The thickness of cross-bed sets often varies with the very local changes in bedform geometry and migration rate that occur in most stream channels (Ethridge and Schumm, 1978). Although the thickness of cross-bed sets, t (m), is less than the original bedform height, h (m), this measured parameter can be used to estimate minimum flow depth, H_{min} (Bridge, 2003):

$$t \approx h \leq 0.4 H_{min}. \quad (22)$$

Cross-beds up to 1 m high were observed, but they were commonly 0.2–0.5 m thick (Fig. 5B), yielding minimum flow depth estimates of 0.5–2.5 m. In sum, the preserved fluvial deposits suggest that flow depth at this site was probably between 1 and 2 m using the methods described above.

4.1.4. Gradient

The paleochannel deposits in this study have been subjected to loading and deformation associated with the Cretaceous Sevier Orogeny and the early Cenozoic Laramide Orogeny, when the San Rafael Swell formed to the west. Regional structural tilt as well as localized faulting has affected paleochannel slope at this site, with faulting primarily effecting the farthest eastern portion of the study region (Doelling, 1994; Lorenz et al., 2006). Topographic data collected near faults or contrary to paleoflow direction were excluded from analysis. The impact of this criterion was the exclusion of data collected near the fault zone in the eastern portion of channel B and the extreme western portion of channel B, where there is a negative upstream slope (Fig. 7). Linear regressions to the longitudinal profiles had good degrees of fit over long-baseline surveys (>1 km). This result was true regardless of channel orientation as channel D is oriented south to north, whereas channel B trends predominantly west to east (Figs. 8 and 9). The slope direction is consistent with paleoflow direction determined by cross-bed orientation, which suggests that aspects of the paleochannel slope have been preserved. The slopes of the ridge surface for channels B and D were 0.0111 (0.64°) and 0.0244 (1.40°), respectively (Figs. 8 and 9).

The issue of reconstructing ancient channel gradients is significant as they are typically low in depositional environments. Since velocity and thus discharge are proportional to $S^{0.5}$ in the micro approach (Eqs. (5) and (6); S is generally not a factor in the macro approach), an order-of-magnitude error in this parameter will affect the discharge estimate by only a factor of ~3, whereas the constraint on width and depth are more important. Here we examine different approaches to estimating paleoslope; in Section 4.2 consistency checks for paleoslope values will be assessed.

Prior studies have reported regional dip values of a few degrees to the north-northeast (e.g., Doelling, 1994; Lorenz et al., 2006). Local faults, especially prevalent in the eastern portion of the study region (Lorenz et al., 2006), prohibit constraining the regional dip to a high degree of accuracy. Field based measurements of a prominent marker bed in the Morrison Formation stratigraphically beneath the Cedar Mountain Formation yielded dip values ranging between 1.5° and 1.9° (0.026 to 0.033), which exceed the magnitude of the measured paleochannel surface slope. Dip direction to the northeast also varied across 25° of azimuth. Assuming that the marker bed was originally horizontal, a reasonable assumption for this lacustrine deposit (Bell, 1986; Currie, 1997, 1998), the corrected paleoslope values would be a few hundredths to a few tenths of a degree (~0.05–0.2°; 0.0009–0.004). However, within the range of measured structural dips were values that resulted in negative channel gradients, reflecting the limitations of this approach due to variable and imprecisely constrained structural dip. We assume a representative value for the regional dip of 1.7°, 35° east of north, which yields reconstructed paleoslope values of 0.001 and 0.002 for channels B and D respectively. These resulting paleoslope values are consistent with slope magnitudes in modern single-thread channels with comparable morphology (shallow slopes of <0.02; Rosgen, 1994).

Paleoslope has been reconstructed for coarse-grained braided rivers based on grain size and flow depth (Paola and Mohrig (1996):

$$S_{est} = (0.094 * D_{50}) / H \quad (23)$$

where S_{est} is the spatially averaged estimate of paleoslope. Paola and Mohrig (1996) report that this method estimates paleoslope to within a factor of 2 with the main sources of error coming from underestimation of depth (leading to overestimation of paleoslope) and overestimation of grain size (leading to underestimation of paleoslope). Derived paleoslope estimates from Eq. (23) (0.001–0.003) are consistent with the values determined from reconstructed paleoslope (gradients of the surveyed channel caprock corrected by a component

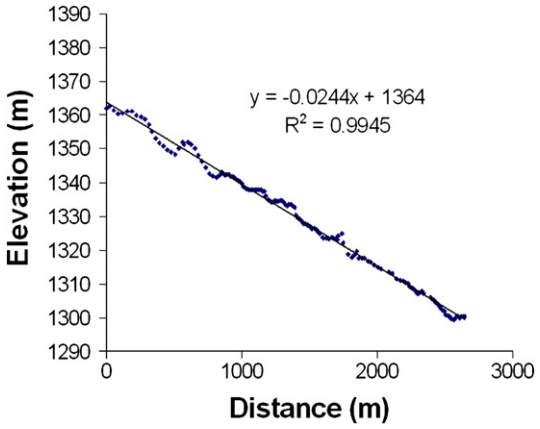

Fig. 9. Longitudinal profile for channel D from south to north. See Fig. 3 for location.

of the NE regional dip) above. However, this method is not applicable to a wide range of fluvial environments, and therefore we did not adopt it in this study.

4.2. Model results

The grain size and overall dimensions between channels B and D are very similar, despite the fact that these two stratigraphically distinct channels were active at different times. Thus, the model results for both channels will be discussed jointly (Table 5). Estimates of threshold flow depths were 1–2 m from Eqs. (3) and (4), although maximum peak flow depths may have been as high as ~10 m (the maximum thickness of the conglomerate caprock) during major flood events. The latter is an upper limit, assuming limited vertical erosion of the caprock after it became re-exposed, as overbank deposition of fines may have offset reductions in channel depth from bed aggradation over time. Velocities associated with threshold flow were between 1.5 and 2.5 m/s, with discharges ranging from 150 to 325 m^3/s (see Table 5 for equations used). Peak discharges for this system were likely higher than the threshold discharge values reported here. Discharge estimates based on channel form ranged from 154 to 493 m^3/s (Table 5). The range of threshold discharge values determined from the micro approach overlaps the field of values determined from the macro approach. This overlap demonstrates consistency in results from two different methodologies: one that models short-term (e.g., individual event) processes that entrained particles (micro approach) and regime-type equations (macro approach) derived from process/form associations developed over longer time scales that average out the vagaries of individual flow events. Given that initial transport of bed load may occur at depths lower than bankfull ($H_t \leq R$), which is linked to several aspects of channel morphometry (Knighton, 1998), it is reasonable that the micro approach generally yielded lower discharge values than the macro approach. The equations applied in this analysis represent a range of fluvial environments, and a much more confined range of plausible discharge values can be identified by selecting those relationships formulated for gravel-bedded streams (e.g., Eqs. (8), (9), (13), and (14)). Notably, in the absence of such knowledge, the overall range of discharge values obtained from all methods employed is well within one order of magnitude.

The plausibility of model results was evaluated in several ways. First-order agreement was good between computed threshold flow depths (from Eqs. (3) and (4)) of 1–2 m and field-based observations of flow conditions preserved in the paleochannel deposits (see Section 4.1.3).

Bedforms are another record of flow conditions. Simons and Richardson (1966) demonstrated with flume data that resistance, expressed as the Darcy–Weisbach friction factor, varies with the type of bedform; in the lower flow regime, f is between 0.042 and 0.16; whereas in the upper flow regime, f is between 0.02 and 0.07. The exhumed channels in this study preserve bedforms (e.g., ripples observed in vertical exposures, Fig. 6C) consistent with lower-flow regime conditions. Consistent with field observations, computed friction factor values (Eqs. (11), (13)–(16)) fall within the lower-flow regime f values advocated by Simons and Richardson, with the exception of the Kleinhans approach (Eq. (16)), which yielded f values in the upper-flow regime. Thus, the results of the Kleinhans approach are not consistent with field observations and should be viewed skeptically in this case.

The validity of paleoflow depth and velocity estimates was assessed by ensuring that the Froude number, F,

$$F = v / \left(g\ H_t\right)^{0.5} \tag{24}$$

remained less than unity. The Froude number is a dimensionless parameter that compares inertial and gravitational forces. In open-channel flow, the nature of the flow (supercritical or subcritical) depends upon whether the Froude number is greater than or less than unity. Subcritical flow ($F<1$) is also consistent with field observations of normal alluvial cross beds in the exhumed paleochannel deposits (e.g., Fig. 6), whereas antidunes (not observed) form in cohesionless sedimentary beds under supercritical flow ($F>1$) conditions (e.g., Bridge, 2003, p. 120). Subcritical flow was considered acceptable for this study based on observed bedforms at the study site and because it is the most common type of flow in natural streams. The maximum Froude value calculated was 0.72, consistent with subcritical flow in all simulations.

Table 5
Estimated paleoflow parameters for selected inverted channel segments in Cedar Mountain Formation, Emery County, Utah.

Paleoflow parameter	Units	Eq.	Channel B	Channel D
Gradient, measured	m/m		0.0111	0.0224
Gradient, corrected	m/m		0.0001	0.002
Channel width	m		58 +/− 14	55 +/− 20
Channel width, used	m		72	75
Ave. max. clast size	mm		16 +/− 4	23 +/− 5
Meander wavelength	m		850	775
Radius of curvature	m		225	150
Flow depth	m	3 + 4	1.8	1.3
Width/depth ratio			40	58
Cross-sectional area	m^2		130	97
n_S		7	0.0196	0.0208
n_L		8	0.0246	0.0263
n_B		9	0.0231	0.0248
n_J		10	0.0210	0.0290
f		11	0.0267	0.0329
f_H		13	0.0399	0.0517
f_G		14	0.0426	0.0560
f_B		15	0.0353	0.0449
f_K		16	0.0624	0.0844
v_S	m/s	5 + 7	2.44	2.56
v_L	m/s	5 + 8	1.94	2.02
v_B	m/s	5 + 9	2.06	2.14
v_J	m/s	5 + 10	2.27	1.84
v_f	m/s	6 + 11	2.33	2.48
v_H	m/s	6 + 13	1.91	1.98
v_G	m/s	6 + 14	1.84	1.90
v_{BA}	m/s	6 + 15	2.02	2.13
v_K	m/s	6 + 16	1.52	1.55
F_S		3 + 5 + 7 + 23	0.57	0.72
F_L		3 + 5 + 8 + 23	0.46	0.57
F_B		3 + 5 + 9 + 23	0.48	0.60
F_J		3 + 5 + 10 + 23	0.53	0.52
F_f		3 + 6 + 11 + 23	0.55	0.70
F_H		3 + 6 + 13 + 23	0.45	0.56
F_G		3 + 6 + 14 + 23	0.43	0.53
F_{BA}		3 + 6 + 15 + 23	0.48	0.60
F_K		3 + 6 + 16 + 23	0.36	0.44
Q_S	m^3/s	2 + 5 + 7	325	248
Q_L	m^3/s	2 + 5 + 8	258	196
Q_B	m^3/s	2 + 5 + 9	275	208
Q_J	m^3/s	2 + 5 + 10	302	178
Q_f	m^3/s	2 + 6 + 11	310	241
Q_H	m^3/s	2 + 6 + 13	254	192
Q_G	m^3/s	2 + 6 + 14	245	185
Q_{BA}	m^3/s	2 + 6 + 15	269	206
Q_K	m^3/s	2 + 6 + 16	203	150
Q_{CA}	m^3/s	17	357	310
Q_{SCH}	m^3/s	18	190	154
Q_{WW}	m^3/s	19	260	274
Q_{WR}	m^3/s	20	493	282
Q_O	m^3/s	21	351	368
Q (mean)			292	228

Subscripts denote use of equations as follows: B = Bray (1979); J = Jarrett (1984); BA = Bathurst (1985); CA = Carlston (1965); f = (Colebrook, 1939); G = Griffiths (1981); H = Hey (1979); L = Limerinos (1970); K = Kleinhans (2005); O = Osterkamp and Hedman (1982); SCH = Schumm (1972); S = Strickler (1923); WW = Williams (1984a, b) Eq. (20); WR = Williams (1984a, b) Eq. (21).

Table 6
Maximum gradient for subcritical flow.

F	Channel B	Channel D
	S (m/m)	S (m/m)
f	0.003	0.004
f_H	0.005	0.006
f_G	0.005	0.007
f_B	0.004	0.006
f_K	0.008	0.01

Substituting the Darcy–Weisbach relationship for threshold velocity (Eq. (5)) into Eq. (24) yields:

$$F = (8S/f)^{0.5}. \quad (25)$$

It is a reasonable assumption that sediment transport did not require supercritical flow conditions in an alluvial channel, so Eq. (25) with computed f values can be used to determine the maximum value of S at $F=1$. The friction factors derived from Eqs. (11) and (13)–(16) range from 0.0267 to 0.0844 and correspond to a range of computed maximum channel gradients from 0.003 to 0.078 for paleochannel B and 0.004 to 0.011 for paleochannel D (Table 6). These maximum gradient values indicate that the field-measured channel gradient (0.0111 and 0.0224) is excessive for the likely subcritical flow conditions that prevailed. In addition, the computed maximum gradient values are larger than the assumed gradients used in the hydraulic models, providing a degree of assurance that reasonable paleoslope values were adopted.

With the micro-approach, maximum discharge values resulted from specific means of estimating roughness within the Manning–Strickler (Eq. (7)) and Darcy–Weisbach (Eq. (11)) approaches, both of which essentially estimate the skin roughness but do not account for other loss factors. Due to their underestimation of the friction factor, these two methods likely overestimate paleodischarge and provide a maximum estimate. Bedform roughness was likely a more important influence on the resistance factor (n or f) in this stream than was grain size. In gravel-bed streams, Bettess (1999) estimated that energy losses in excess of skin roughness can be up to ~50% of that from skin friction based on his analysis of data collected by Griffiths (1981). Formulations for the friction factor based on empirical data (e.g., Eqs. (8)–(10), (13)–(16)) provide a more realistic approximation of frictional dissipation factors in natural rivers to account for additional sources of energy loss (e.g. due to bedform roughness, channel bends etc.) and tend to yield higher friction factor values than Eq. (7) or (11). The net effect of these more realistic, higher friction factors is a correspondingly lower computed discharge value.

As expected, the macro approach yielded discharge values that were generally slightly higher than those derived from the micro approach. Most of the macro approach relationships were derived from fluvial systems where the largest particles were finer grained (clay to sand) than the gravel clasts observed in the Utah exhumed paleochannels. Osterkamp and Hedman (1982) subdivided their data based on median (D_{50}) sediment size and obtained regression relationships for discharge (Q_2) as a function of channel width (their Table 2). Computed discharge varies considerably depending on bed sediment size for a constant channel width as illustrated on the right-hand side of Fig. 10. The largest discharges occur in fine-grained bed material and decrease as the sandiness of the channel bed material increases. This trend is reversed once the median particle size on the channel bed exceeds 2 mm from armoring. Eq. (21), which yielded the highest discharge value for inverted channel D, was derived from their entire data set and matches closely the relationships obtained for sand-bed channels with silt to sand banks, where the majority of their measurements were made. Importantly, their relationship for gravel beds, the median grain size for the exhumed channels in this study, is more consistent with discharge values obtained from the micro-analysis methods than the value obtained from Eq. (21). In addition to the grain size on the channel bed, bank material properties are also a control on discharge, with larger discharges associated with resistant, cohesive (typically clay-rich) banks (Schumm, 1963). Coarse-grained streams with weak channel banks tend to be wide and shallow, with lower discharge per unit width (right-hand side of Fig. 10). The paleochannels examined in this study formed in a substrate that was rich in fines that likely afforded significant bank strength. Overall, this example illustrates that more realistic discharge values are obtained when hydraulic equations applicable to a given fluvial environment are used.

We assessed the impact of uncertainty in input parameter values on computed discharge values. In this study, grain size was the best-constrained parameter, with coarse gravels as the maximum clast size measured at multiple sample sites. Errors also arose from determining channel width from preserved channel fragments, as discussed above. The former energy gradient was approximated by a first-order structural correction to the modern channel surface slope. Thus, this parameter probably represents the greatest source of error in the paleoflow computations. A range of paleoslope values from the measured values (few hundreths) to the reconstructed values (few thousandths) were assessed in the paleohydrologic models. This range of values also coincides with the plausible range of energy gradients for this type of gravel bed meandering river. Using the uncorrected channel slopes (measured values of a few tenths) yielded threshold flow depths of a few tens of centimeters and discharge values from the micro-approach of tens of cubic meters per second. These model-derived results may represent low flow conditions, but these modest flows were not responsible for the bulk of the geomorphic work and construction of the overall channel form. Several of the models yielded Froude numbers greater than unity, a result inconsistent with field observations that support subcritical flow conditions and flow depths of a few meters. Utilizing the reconstructed paleoslope values, computed flow depths of 1–2 m and paleodischarge values of a few hundred cubic meters per second were obtained, in good agreement with field observations. Slopes an order of magnitude greater than those measured in the field (few tenths, equivalent to very steep rivers) were evaluated and produced unrealistic model-derived results (i.e., $H_t << 0.1$ m and $V_t \sim 0$ m/s). Overall, this analysis suggests that the corrected paleoslope values (0.001–0.002) used in this study are reasonable.

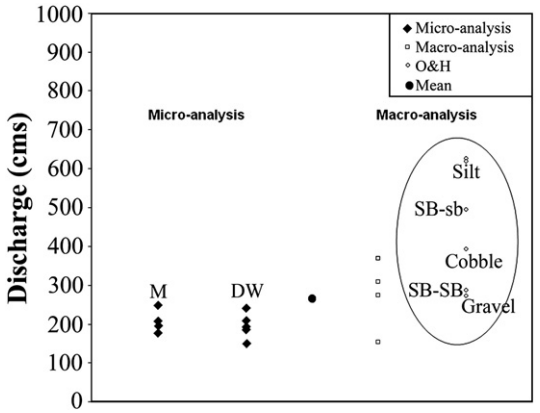

Fig. 10. Computed discharges from multiple models for channel D are plotted with arbitrary offset on the x-axis for clarity. The mean value is from the models evaluated in this study (see text for details). Discharge values obtained from the Osterkamp and Hedman (1982) equations based on channel width (here assumed to be 75 m) and median grain size, enclosed in oval, illustrate the effect of bed material size on discharge. [These values were not included in the computation of the mean.] Discharges obtained from relationships for the coarser bed material agree well with discharge obtained from other methods in this study. Abbreviations: M = Manning, DW = Darcy–Weisbach, O&H = Osterkamp and Hedman, SB-sb = sand-bed, silt-bank, SB-SB = sand-bed, sand-bank.

Computed discharge values were found to vary significantly according to the variability of the input parameters. For example, by varying grain size by up to one standard deviation on either side of the mean, varying width by one standard deviation from the third quartile value, and varying slope by ±50% of the assumed value as a conservative estimate resulted in discharge differences of up to ±60%, ±33%, and ±227%, respectively. Varying multiple variables generally results in discharge estimates within a factor of 2. Assuming a 10% sediment concentration (Eq. (4)) in the flow (i.e., 1165 kg/m^3 total fluid density), a high value for this type of river, produced a modest reduction in the model discharge values by up to 20%. However, we should note that these results still yielded discharge values of comparable magnitude to the original discharge estimates in the vast majority of cases.

5. Discussion

The approach adopted in this study yields an envelope of discharge values, an indication of the plausible range as verified through field observations. The overall mean discharge value tended toward the maximum value in the micro approach and an intermediate value for the macro approach. When evaluating the paleohydraulics of the system, considering both approaches is desirable and important to mitigate uncertainties in each variable and take full advantage of the available data. None of the individual methods used can be expected to provide very precise results, but taken together they do indicate the order of magnitude of paleovelocity and paleodischarge. More realistic discharge values are obtained when hydraulic equations applicable to a given fluvial environment are used. In the case where only landform shape attributes are known from remotely sensed data, the macro approach can be applied, which yields generally higher discharge values than the micro approach and reflects the long-term equilibrium balance within the system.

Application of these models to martian sinuous ridges is likely to also yield a plausible range of paleodischarge values; however, several noteworthy differences relative to the exhumed paleochannels in Utah are discussed here. First, inferred inverted channels on Mars may have developed as a result of alternative indurating agents. In addition to cements (most likely ferricrete or sulfates, or potentially chlorides on Mars; Landis et al., 2004, Bibring et al., 2005, 2006; Osterloo et al., 2008), clast armoring or lava infilling can act to inhibit erosion and lead to inverted topography. On the basis of channel form alone, no diagnostic indicator of the indurating agent is recognized, but aspects of the preserved form can suggest that one mechanism was more likely than another. For example, weathering of competent blocks of the caprock due to undermining is characteristic of cemented fluvial deposits (Fig. 4). In addition, the geologic setting and regional context (e.g., source regions for lava flows) are important clues in assessing various indurating agents for martian sinuous ridges.

Cementation and clast armoring are two processes that have the potential to preserve the entire (or nearly entire) fluvial system, whereas lava flows may only inundate a reach of the network. Thus, lower-order tributaries located at higher elevations in the drainage system may not be preserved in the case of lava infilling, or a lava flow may not extend to higher-order segments downslope. However, individual conditions within a given fluvial system affect the preservation. The main trunk channels are preserved in the exhumed, cemented paleochannels discussed in this study, and branches are preserved less frequently (Fig. 4C). This planimetric form may reflect the original network pattern, efficacy of modern erosion at removing smaller channels, and/or variations in the availability and concentration of cement constituents within the network.

The best preservation of the original channel form results from cementation or clast armoring. In addition, these processes can also preserve sedimentary structures, such as meander scroll bars or trough cross beds, which would be obscured by lava flows. Lavas flowing into a valley can fill the original fluvial channel as well as the larger valley, resulting in the potential for an overestimation of channel width.

Second, differences exist in the certainty of input parameter values. In contrast to the terrestrial analog, grain size is the least-constrained parameter for martian sinuous ridges, as direct in situ measurements are only available at a few locations on Mars where spacecraft have landed, none of which is a sinuous ridge site. Inference of grain size from thermal data is hampered in many areas by the pervasive dust layer (Presley and Christensen, 1997). Orbital image data are limited to resolutions $>\sim$1 m/pixel in visible wavelengths using HiRISE images (McEwen et al., 2007). Howard et al. (2007) interpreted meter-scale boulders on inverted channels in Eberswalde crater to be flood-transported material and a primary depositional feature. However, boulders have not been observed on the bulk of sinuous ridges observed to date. We can reasonably assume that sand and gravel size particles comprise the maximum grain size for most sinuous ridges; however, even this range in grain size (0.25–64 mm) has significant impact on the model results.

The original channel slope may be largely preserved on Mars. In the absence of plate tectonics, and with the large-scale topographic shape associated with volcanic loading in Tharsis established early in the planet's history (Phillips et al., 2001), factors that could alter channel slope include impact cratering and subsidence or compaction from overburden, as many of the martian sinuous ridges show evidence of past burial (e.g., Williams, 2007). Subsequent exhumation of martian sinuous ridges was presumably done by aeolian as opposed to dominantly fluvial erosion (Williams et al., 2007). Slopes on Mars can be determined from global Mars Orbiter Laser Altimeter (MOLA) topographic data (150 m shot size, with shot-to-shot spacing of 300 m; Smith et al., 2001; Neumann et al., 2001) or from digital elevation models derived from meter and submeter-scale stereo images of specific sites (e.g., McEwen et al., 2007; Malin et al., 2007; Ansan et al., 2008).

Finally, the models must account for the lower gravitational acceleration on Mars. Gravity scaling of the micro approach is straightforward (see, e.g., Komar, 1979). However, gravity is not an explicit term in the empirical macro approach, and the lower martian gravity would yield greater channel width, depth, and meander wavelength per unit discharge than on Earth. Relationships between these factors also depend on the unknown strength of the bank material, which affects the w/H ratio. The uncorrected macro approach would overestimate the Martian discharge values by a factor of 1.61 (Irwin et al., 2008). Given the variability of paleodischarge values obtained from the individual methods, the resultant envelope of values is likely to incorporate the actual paleodischarge value. Further study of these inverted fluvial systems on Earth will help to elucidate the magnitude and relative timing of fluvial activity on Mars.

6. Conclusions

Cemented paleochannel deposits, now exposed as ridge forms because of landscape inversion, preserve key attributes of the former fluvial environment. A record of the fluvial conditions during active flow is preserved, such as original channel shape (preserved in some sections), flow direction, and sediment transport capability. Paleochannel dimensions, slope, and grain size distribution can be used to estimate paleoflow conditions using paleohydraulic models. The 14 paleohydraulic models evaluated in this study yield an envelope of plausible discharge values that are well within an order of magnitude. Field observations and computed Froude numbers confirmed that reasonable paleoflow values were derived from the models assessed. Those methods based on the physics of transporting the coarser component of sediment (micro approach) generally produced lower estimates of dominant discharge than discharge-form relations (macro approach) as sediment transport may be initiated at

discharges below bankfull. In addition, models used in the macro approach were largely developed based on fluvial systems with finer sediment than the gravel-bedded examined here. The range of discharge values can be narrowed when numeric models derived from comparable fluvial environments are used. The results of this study demonstrate the validity of applying empirically and theoretically derived paleohydrologic models to inverted channels, including inferred similar landforms on Mars.

Acknowledgements

The authors are grateful to A. Johnston (Smithsonian Institution) for technical advice, T. Chidsey (Utah Geologial Survey) and Brian S. Curie (Miami University-Ohio) for information regarding the study site, and Doug Cox for development of USAPhotoMaps. This manuscript was improved by comments of V. Baker, G. Komatsu, A. Howard and two anonymous reviewers. This research was supported by a NASA Mars Fundamental Research Grant #NNX06AB21G and a research grant from the Becker Endowment from the Smithsonian Institution awarded to R.M.E. Williams. This is Planetary Science Institute contribution #444.

References

Ansan, V., Mangold, N., Masson, P., Gailhardis, E., Neukum, G., 2008. Topography of valley networks on Mars from Mars Express High Resolution Stereo Camera digital elevation models. Journal of Geophysical Research 113 (E7), E07006.

Arakel, A.V., 1986. Evolution of calcrete in paleodrainages of the Lake Napperby Area, central Australia. Palaeogeography, Palaeoclimatology, Palaeoecology 54, 283–303.

Arcement, G.J., Schneider, V.R., 1989. Guide for Selecting Manning's Roughness Coefficients for Natural Channels and Flood Plains—Metric Version. U.S. Geological Survey Water-supply Paper 2339, Washington, D.C. 67 pp.

Al-Suwaidi, A.H., Gonzalez, L.A., Ludvigson, G.A., Tremain, E., 2007. When Carbonates Speak: Reconstructing Mid-Cretaceous Paleoclimate and Paleoenvironment from Carbonates in the Ruby Ranch Member of the Cedar Mountain Formation. GSA Abstracts with Programs, vol. 39, p. 40.

Bathurst, J.C., 1985. Flow resistance estimation in mountain rivers. Journal Hydraulic Engineering, American Association of Civil Engineers 111, 625–643.

Bell, T.E., 1986. Deposition and diagenesis of the Brushy Basin Member and upper part of the Westwater Canyon Member of the Morrison Formation, San Juan Basin, New Mexico. In: Turner-Peterson, C.E., Santos, E.S., Fishman, N.S. (Eds.), A basin analysis case study: The Morrison Formation Grants uranium region New Mexico: American Association of Petroleum Geologists Studies in Geology, vol. 22, pp. 1847–1866.

Bettess, R., 1999. Flow resistance equations for gravel bed rivers. Proceedings 27th IAHR Congress, Volume CDROM, part E, Graz, Austria, p. 6.

Bhattacharya, J.P., Payenberg, T.H.D., Lang, S.C., Bourke, M., 2005. Dynamic river channels suggest a long-lived Noachian crater lake on Mars. Geophysical Research Letters 32 (10), L10201.

Bibring, J.P., Gendrin, A., Gondet, G., Poulet, F., Berthe, M., Soufflot, A., Arvidson, R., Mangold, N., Mustard, J., Drossart, P., OMEGA team, 2005. Mars surface diversity as revealed by the OMEGA/Mars Express observations. Science 307, 1576–1581.

Bibring, J.P., Langevin, Y., Mustard, J.F., Poulet, F., Arvidson, R., Gendrin, A., Gondet, B., Mangold, N., Pinet, P., Forget, F., OMEGA team, 2006. Global mineralogical and aqueous Mars history derived from OMEGA/Mars Express data. Science 312, 400–404.

Bray, D.I., 1979. Estimating average velocity in gravel-bed rivers. Journal of the Hydraulic Division, ASCE 105, 1103–1122.

Bridge, J.S., 2003. Rivers and Floodplains. Blackwell Publishing, Malden, MA, pp. 104–115.

Burr, D.M., Williams, R.M.E., Nussbaumer, J., Zimbelman, J.R., 2006. Multiple, distinct, (glacio?)fluvial paleochannels throughout the western Medusae Fossae Formation, Mars. Lunar and Planetary Sci. Conf. XXXVII, p. 1367. Abstract.

Burr, D.M., Enga, M.T., Williams, R.M.E., Zimbelman, J.R., Howard, A.D., Brennand, T.A., 2008. Pervasive aqueous paleoflow features in the Aeolis/Zephyria Plana region, Mars. Icarus. doi:10.1016/j.icarus.2008.10.014.

Carlston, C.W., 1965. The relation of free meander geometry to stream discharge and its geomorphic implications. American Journal of Science 263, 864–885.

Church, M., 1978. Palaeohydrological reconstructions from a Holocene valley fill. In: Miall, A.D. (Ed.), Fluvial Sedimentology 743–772.

Church, M., 1992. Channel morphology and topology. In: Calow, P., Petts, G.E. (Eds.), The Rivers Handbook. Blackwell, Oxford, UK, pp. 126–143.

Colby, B.R., 1964a. Discharge of sands and mean–velocity relationships in sand-bed streams. U.S. Geological Survey Professional Paper 462-A. 47 pp.

Colby, B.R., 1964b. Scour and fill in sand-bed streams. U.S. Geological Survey Professional Paper 462-D. 32 pp.

Colebrook, C.F., 1939. Turbulent flow in pipes, with particular reference to the transition region between smooth and rough pipe laws. Journal Institution of Civil Engineers, London 11, 133.

Colebrook, C.F., White, C.M., 1937. Experiments with fluid friction in roughened pipes. Proceedings of the Royal Society of London, Series A, vol. 161, pp. 367–387.

Currie, B.S., 1997. Sequence stratigraphy of nonmarine Jurassic–Cretaceous rocks, central Cordilleran foreland-basin system. Geological Society of America Bulletin 109 (9), 1206–1222.

Currie, B.S., 1998. Upper Jurassic–Lower Cretaceous Morrison and Cedar Mountain Formation, NE Utah–NW Colorado: relationships between nonmarine deposition and early Cordilleran foreland-basin development. Journal of Sedimentary Research 68 (4), 632–652.

Davis, S.W., et al., 2001. Erosional history of the Colorado River through Glen and Grand Canyons. In: Young, R.A., Spamer, E.E. (Eds.), Colorado River origin and evolution—Proceedings of a symposium held at grand Canyon National Park in June, 2000. Grand Canyon Association, pp. 135–139.

Demko, T.M., Currie, B.S., Nicoll, K.A., 2004. Regional paleoclimatic and stratigraphic implications of paleosols and fluvial/overbank architecture in the Morrison Formation (Upper Jurassic), Western Interior, USA. Journal of Sedimentary Geology 167, 115–135.

Doelling, H., 1994. Tufa deposits in western Grand County. Survey Notes—Utah Geological Survey 26, 8–10.

Ethridge, F.G., Schumm, S.A., 1978. Reconstructing paleochannel morphology and flow characteristics: methodology, limitations, and assessment. In: Miall, A.D. (Ed.), Fluvial sedimentology, Canadian Society Petroleum Geologists Memoir 5, pp. 703–722. doi:10.1002/esp.3760050213.

Elder, W.P., Kirkland, J.I., 1993. Cretaceous paleogeography of the Colorado Plateau and adjacent areas. In: Morales, M. (Ed.), Aspects of Mesozoic geology and paleontology of the Colorado Plateau, vol. 59. Museum of Northern Arizona Bulletin, Flagstaff, AZ, pp. 129–151.

Fassett, C.I., Head III, J.W., 2005. Fluvial sedimentary deposits on Mars: ancient deltas in a crater lake in the Nili Fossae region. Geophysical Research Letters 32, L14201. doi:10.1029/2005GL023456.

Gioia, G., Bombardelli, F.A., 2002. Scaling and Similarity in Rough Channel Flows. Physical Review Letters 88 (4), 014501. doi:10.1103/PhysRevLett.88.014501.

Griffiths, G.A., 1981. Flow resistance in coarse gravel bed rivers, Proc. ASCE, Journal of Hydraulic Division 107 (7), 899–918.

Hanks, T.C., et al., 2001. The Colorado River and the age of Glen Canyon. In: Young, R.A., Spamer, E.E. (Eds.), Colorado River origin and evolution—Proceedings of a symposium held at grand Canyon National Park in June, 2000. Grand Canyon Association, pp. 129–133.

Harris, D.R., 1980. Exhumed Paleochannels in the Lower Cretaceous Cedar Mountain Formation Near Green River, Utah. Brigham Young University Geology Studies, vol. 27, pp. 51–66. Salt Lake City, UT.

Hey, R.D., 1979. Flow resistance in gravel-bed rivers, Proc. ASCE. Journal of Hydraulics Division 105 (4), 365–379.

Howard, A.D., 1981. Etched plains and braided ridges of the south polar region of Mars: features produced by basal melting of ground ice? Reports of the Planetary Geology Program, NASA TM 84211, Washington, D.C. , pp. 286–288.

Howard, A.D., Moore, J.M., Irwin III, R.P., Dietrich, W.E., 2007. Boulder transport across the Eberswalde delta. Lunar Planetary Sci. Conf. XXXVIII, p. 1168. Abstract.

Irwin, R.P., III Craddock, R.A., Howard, A.D., 2005. Interior channels in Martian valley networks: discharge and runoff production. Geology 336, 489–492.

Irwin III, R.P., Howard, A.D., Craddock, R.A., 2008. Fluvial valley networks on Mars. In: Rice, S., Roy, A., Rhoads, B. (Eds.), River Confluences and the Fluvial Network. John Wiley and Sons, West Sussex, U.K., pp. 409–430.

Jarrett, R.D., 1984. Hydraulics of high gradient streams. Journal of Hydraulic Engineers 110, 1519–1539.

Jerolmack, D.J., Mohrig, D., Zuber, M.T., Byrne, S., 2004. A minimum time for the formation of Holden Northeast fan, Mars. Geophysics Research Letters 31, L21701. doi:10.1029/2004GL021326.

Jopling, A.V., 1966. Some procedures and techniques used in reconstructing the hydraulic parameters of a paleoflow regime. Journal of Sedimentary Petrology 36, 5–49.

Kargel, J.S., Strom, R.G., 1992. Ancient glaciation on Mars. Geology 20, 3–7.

Keulegan, G.H., 1938. Laws of turbulent flow in open channels. J. Res. Natl. Bur. Stand. 21, Paper 1151, Washington, DC, pp. 707–741.

Khalaf, F.I., 1990. Occurrence of phetic dolocrete within Tertiary clastic deposits of Kuwait, Arabian Gulf. Sedimentary Geology 80, 223–239.

Kirkland, J.I., Lucas, S.G., Estep, J.W., 1998. Cretaceous dinosaurs of the Colorado Plateau. In: Lucas, S.G., Kirkand, J.I., Estep, J.W. (Eds.), Lower and middle Cretaceous terrestrial ecosystems: New Mexico Museum of Natural History and Science Bulletin No. 14, Albuquerque, NM, pp. 79–89.

Kleinhans, M.G., 2005. Flow discharge and sediment transport models for estimating minimum timescale of hydrological activity and channel and delta formation on Mars. Journal of Geophysical Research 110, E12003. doi:10.1029/2005JE002521.

Knighton, D., 1998. Fluvial Forms and Processes: A New Perspective. Oxford Univ. Press, New York. 338 pp.

Komar, P.D., 1979. Comparisons of the hydraulics of water flows in martian outflow channels with flows of similar scale on Earth. Icarus 37, 156–181.

Komar, P.D., 1988. Sediment transport by floods. In: Baker, V.R., Kochel, R.C., Patton, P.C. (Eds.), Flood geomorphology. Wiley-Interscience, New York, pp. 97–111.

Krumbein, W.C., Sloss, L.L., 1963. Stratigraphy and Sedimentation, 2nd edition. Freeman, San Francisco. 660 pp.

Landis, G.A., Blaney, D., Cabrol, N., Clark, B.C., Farmer, J., Grotzinger, J., Greeley, R., Richter, L., Yen, A., the MER Athena Science Team, 2004. Transient liquid water as a mechanism for induration of soil crusts on Mars. Lunar and Planetary Science Conf. XXXV, p. 2188. Abstract.

Langbein, W.B., Leopold, L.B., 1964. Quasi-equilibrium states in channel morphology. American Journal of Science 262, 782–794.

Limerinos, J.T., 1970. Determination of the Manning coefficient from measured bed roughness in natural channels. USGS Water-Supply Paper 1898B. 47 pp.

Liu, H.K., Hwang, S.Y., 1959. Discharge formula for straight alluvial channels. ASCE, Journal Hydraulics Division, ASCE, 85 (HY11) Proc. Paper 2260, pp. 65–97.
Livesey, R.H., 1963. Channel armoring below Fort Randall Dam. Miscellaneous publication — United States Department of Agriculture 970, 461–469.
Lorenz, J.C., Cooper, S.P., Olsson, W.A., 2006. Natural fracture distributions in sinuous, channel-fill sandstones of the Cedar Mountain Formation, Utah. Americna Association of Petroleum Geologists Bulletin 90 (9), 1293–1308.
Maizels, J.K., 1983. Palaeovelocity and palaeodischarge determination for coarse gravel deposits. In: Gregory, K.J. (Ed.), Background to paleohydrology: A Perspective. John Wiley and Sons, New York, pp. 101–139.
Maizels, J.K., 1987. Plio-Pleistocene raised channel systems of the western Sharqiya (Wahiba), Oman. In: Frostick, L., Reid, L. (Eds.), Desert Sediments: Ancient and Modern. Geological Society Special Publication, pp. 31–50.
Malin, M.C., et al., 2007. Context Camera Investigation on board the Mars Reconnaissance Orbiter. Journal of Geophysical Research 112, EO5S04.
Malin, M.C., Edgett, K.S., 2001. Mars Global Surveyor Mars Orbiter Camera: interplanetary cruise through primary mission. Journal of Geophysical Research 106 (E10), 23,429–23,570.
Malin, M.C., Edgett, K.S., 2003. Evidence for persistent flow and aqueous sedimentation on early Mars. Science 302, 1931–1934. doi:10.1126/science.1090544.
Malin, M.C., Danielson, G.E., Ingersoll, A.P., Masursky, H., Veverka, J., Ravine, M.A., Soulanille, T.A., 1992. The Mars Observer Camera. Journal of Geophysical Research 97 (E5), 7699–7718. doi:10.1029/92JE00340.
Malin, M.C., Carr, M.H., Danielson, G.E., Davies, M.E., Hartmann, W.K., Ingersoll, A.P., James, P.B., Masursky, H., McEwen, A.S., Soderblom, L.A., Thomas, P., Veverka, J., Caplinger, M.A., Ravine, M.A., Soulanille, T.A., Warren, J.L., 1998. Early views of the martian surface from the Mars Orbiter Camera of Mars Global Surveyor. Science 279, 1681–1685. doi:10.1126/science.279.5357.1681.
Mangold, N., Quantin, C., Ansan, V., Delacourt, C., Allemand, P., 2004. Evidence for precipitation on mars from dendritic valleys in the Valles Marineris Area. Science 305, 78–81. doi:10.1126/science.1097549.
Marchetti, D.W., Cerling, T.E., 2001. Bedrock incision rates for the Fremont River tributary of the Colorado River. In: Young, R.A., Spamer, E.E. (Eds.), Colorado River origin and evolution—Proceedings of a symposium held at grand Canyon National Park in June, 2000. Grand Canyon Association, pp. 125–127.
McCauley, J.F., et al., 1972. Preliminary Mariner 9 report on the geology of Mars. Icarus 17, 289–327.
McEwen, A.S., Eliason, E.M., Bergstrom, J.W., Bridges, N.T., Hansen, C.J., Delamere, W.A., Grant, J.A., Gulick, V.C., Herkenhoff, K.E., Keszthelyi, L., Kirk, R.L., Mellon, M.T., Squyres, S.W., Thomas, N., Weitz, C.M., 2007. MRO's High Resolution Imaging Science Experiment (HiRISE). Journal of Geophysical Research 112, E05S02. doi:10.1029/2005JE002605.
McMenamin, D.S., McGill, G.E., 2005. Processes involved in the formation of Martian fan-shaped deposits. Lunar and Planetary Science Conf. XXXVI, p. 1732. Abstract.
Moore, J.M., Howard, A.D., 2005. Large alluvial fans on Mars. Journal of Geophysical Research 110, E04005. doi:10.1029/2004JE002352.
Moore, J.M., Howard, A.D., Dietrich, W.E., Schenk, P.M., 2003. Martian layered fluvial deposits: implications for Noachian climate scenarios. Geophysical Research Letters 30 (24), 2292. doi:10.1029/2003GL019002.
Neumann, G., Rowlands, D., Lemoine, F., Smith, D., Zuber, M., 2001. Crossover analysis of Mars Orbiter Laser Altimeter data. Journal of Geophysical Research 106 (E10), 23753–23768.
Nuccio, V.F., Condon, S.M., 1996. Burial and thermal history of the Paradox basin, Utah and Colorado, and petroleum potential of the Middle Pennsylvanian Paradox Formation. U.S. Geological Survey Bulletin 2000-O 41 pp.
Nuccio, V.F., Roberts, L.N.R., 2003. Chapter 4—Thermal maturity and oil and gas generation history of petroleum systems in the Uinta–Piceance province, Utah and Colorado. Petroleum systems and geologic assessment of oil and gas in the Uinta–Piceance province, Utah and Colorado, U.S. Geological Survey Digital Data Series, DDS-69-B, Denver, CO. 39 pp.
Nussbaumer, J., Jaumann, R., Hauber, E., 2003. Evidence for a surging ice-sheet in Elysium Planitia, Mars. Sixth International Conference on Mars, p. 3018. Abstract.
Osterkamp, W.R., Hedman, E.R., 1982. Perennial-streamflow characteristics related to channel geometry and sediment in Missouri River basin. U.S. Geological Survey Professional Paper 1242. 37 pp.
Osterloo, M.M., et al., 2008. Chloride-bearing materials in the Southern Highlands of Mars. Science 319, 1651–1654.
Parker, G., Klingeman, P.C., McLean, D.L., 1982. Bedload and size distribution in paved gravel-bed streams. Journal of Hydraulic Engineering 108, 544–571.
Pain, C.F., Ollier, C.D., 1995. Inversion of relief—a component of landscape evolution. Geomorphology 12, 151–165.
Pain, C.F., Clarke, J.D.A., Thomas, M., 2007. Inversion of relief on Mars. Icarus 190 (2), 478–491. doi:10.1016/j.icarus.2007.03.017.
Paola, C., Borgman, L., 1991. Reconstructing random topography from preserved stratification. Sedimentology 38, 553–565.
Paola, C., Mohrig, D., 1996. Palaeohydraulics revisited: palaeoslope estimation in coarse-grained braided rivers. Basin Research 8, 243–254.
Pederson, J., Karlstrom, K., Sharp, W., McIntosh, W., 2002. Differential incision of the Grand Canyon related to Quaternary faulting—constraints from U-series and Ar/Ar dating. Geology 30 (8), 739–742.
Phillips, R.J., et al., 2001. Ancient geodynamics and global-scale hydrology on Mars. Science 291 (5513), 2587–2591.
Presley, M.A., Christensen, P.R., 1997. Thermal conductivity measurements of particulate materials 2. Results. Journal of Geophysical Research 102 (E3), 6551–6566.
Raudkivi, A.J., 1967. Loose Boundary Hydraulics. Pergamon Press, Oxford, United Kingdom,. 331 pp.
Rosgen, D., 1994. A classification of natural rivers. Catena 22, 169–199.
Sahagian, D., Proussevitch, A., Carlson, W., 2002. Timing of Colorado Plateau uplift: initial constraints from vesicular basalt-derived paleoelevations. Geology 30 (9), 807–810.
Schumm, S.A., 1963. A tentative classification of alluvial river channels. U.S. Geological Professional Circuclar, p. 477.
Schumm, S.A., 1972. Fluvial paleochannel, In: Rigby, J. K. & Hamblin W. K. (Eds), Recognition of Ancient Sedimentary Environments. Society of Economic Paleontologists and Mineralogist, Special Publication 16, Tulsa, OK, pp. 179–183.
Sharp, R.P., 1973. Mars: south polar pits and etched terrain. Journal of Geophysical Research 78, 4222–4230.
Shields, A., 1936. Application of similarity principles and turbulence research to bed-load Movement. Translated into English by: Ott, W.P. and Unchelen, J.C. (Translators), Mitteilungen der preussischen Nersuchsanstalt fur Wassed Brau end Schiffbuar. Report 167, California Institute of Technology, Pasedena, California.
Shipton, Z.K., Evans, J.P., Kirschner, D., Kolesar, P.T., Williams, A.P., Heath, J., 2004. Analyses of CO_2 leakage through "low-permeability" faults from natural reservoirs in the Colorado Plateau, east-central Utah. In: Baines, S.J., Worden, R.H. (Eds.), Geological storage of carbon dioxide. Geological Society (London) Special Publications, vol. 233, pp. 43–58.
Silberman, E., Carter, R.W., Einstein, H.A., Hinds, J., Powell, R.W., 1963. Friction Factors in Open Channels, Progress Report of the Task Force on Friction Factors in Open Channels of the Committee of Hydromechanics of the Hydraulics Division. Proceedings of the American Society of Civil Engineers, Journal of Hydraulics Division, ASCE, 89 (HY2) Proc. Paper 3464, pp. 97–143.
Simons, D.B., Richardson, E.V., 1966. Resistance to flow in alluvial channels. U.S. Geological Survey Professional Paper, 422J. 61 pp.
Smith, D.E., et al., 2001. Mars Orbiter Laser Altimeter: experiment summary after the first year of global mapping of Mars. Journal of Geophysical Research 106 (E10), 23,689–23,722.
Soderblom, L.A., Dreidler, T.J., Masursky, H., 1973. Latitudinal distribution of a debris mantle on the martian surface. Journal of Geophysical Research 78, 4117–4122.
Spötl, C., Writght, V.P., 1992. Groundwater dolocretes from the Upper Triassic Paris basin, France: a case study of an arid, continental diagenetic facies. Sedimentology 39, 1119–1136.
Stokes, W.L., 1961. Fluvial and eolian sandstone bodies in the Colorado Plateau. In: Petersen, J.A., Osmond, J.C. (Eds.), Geometry of sandstone bodies. American Association of Petroleum Geologists Bulletin, pp. 151–178.
Strickler, A., 1923. Beiträge zur Frage der Geschwindigkeits - formel und der Rauhigkeitszamen für Ströme, Kanäle, und geschlossene Leitungen. Mitteil. Des Amtes für Wasserwirtschaft, Bern. No. 16, 77 pp. Translated into English by: Roesgan, T. and Brownlie, W.R., 1981, Contributions to the Question of a Velocity Formula and Roughness data for Streams, Channels and Closed Pipelines, Translation No. T-10. Pasadena, CA: California Institute of Technology, W.M. Keck Laboratory of Hydraulics and Water Resources.
Thorne, C.R., Zevenbergen, L.W., 1985. Estimating mean velocity in mountain rivers. Journal of Hydraulic Engineering, American Society of Civil Engineers 111, 612–624.
Wentworth, C.K., 1922. A scale of grade and class terms for clastic sediments. Journal of Geology 30, 377–392.
Williams, G.P., 1984a. Palaeohydrological equations for rivers. In: Costa, J.E., Fleisher, P.J. (Eds.), Developments and Applications of Geomorphology. Springer-Verlag, New York, pp. 343–367.
Williams, G.P., 1984b. Palaeohydrological methods and some examples from Swedish fluvial environments. II. River meanders. Geografska Annaler 66A, 89–102.
Williams, R.M.E., 2007. Global spatial distribution of raised curvilinear features on Mars. Lunar and Planetary Science Conf. XXVIII, p. 1821. Abstract.
Williams, P.E., and Hackman, R.J., 1971. Geology of the Salina quadrangle, Utah: U. S. Geological Survey map I-591-A, miscellaneous investigations series, scale 1:250,000, 1 sheet, reprinted 1983.
Williams, R.M.E., Edgett, K.S., 2005. Valleys in the martian rock record. Lunar and Planetary Science Conf. XXXVI, p. 1099. Abstract.
Williams, R.M.E., Malin, M.C., Edgett, K.S., 2005. Remnants of the courses of fine-scale, precipitation-fed runoff streams preserved in the martian rock record. Lunar and Planetary Science Conf. XXXVI, p. 1173. Abstract.
Williams, R.M.E., Chidsey Jr., T.C., Eby, D.E., 2007. Exhumed paleochannels in central Utah — analogs for raised curvilinear features on Mars. In: Willis, G.C., Hylland, M.D., Clark, D.L., ChidseyJr. Jr., T.C. (Eds.), Central Utah — diverse geology of a dynamic landscape: Utah Geological Association Publication 36, Salt Lake City, Utah, pp. 220–235.
Willis, G.C., Biek, R.F., 2001. Quaternary incision rates of the Colorado River and major tributaries in the Colorado Plateau. In: Young, R.A., Spamer, E.E. (Eds.), Colorado River origin and evolution—Proceedings of a symposium held at grand Canyon National Park in June, 2000. Grand Canyon Association, pp. 119–123.
Wohl, E., 2000. Mountain Rivers. Water Resources Monograph 14. American Geophysics Union, Washington, D.C., pp. 70–85.
Wolman, M.G., 1954. A method of sampling coarse river-bed material. Transactions of the American Geophysical Union 35 (6), 951–956.
Wood, L.J., 2006. Quantitative geomorphology of the Mars Eberswalde delta. Geological Society of America Bulletin 118, 557–566. doi:10.1130/B25822.1.
Yingling, V.L., Heller, P.L., 1992. Timing and record of foreland sedimentation during the initiation of Sevier orogenic belt in central Utah. Basin Research 4, 279–290.